




TANSPEC: TIFR-ARIES Near-infrared Spectrometer

Saurabh Sharma¹ , Devendra K. Ojha², Arpan Ghosh¹, Joe P. Ninan², Supriyo Ghosh², Swarna K. Ghosh², P. Manoj², Milind B. Naik², Savio L. A. D'Costa², B. Krishna Reddy¹, Nandish Nanjappa¹, Rakesh Pandey¹, Tirthendu Sinha¹, Neelam Panwar¹, Susmitha Antony^{2,3}, Harmeen Kaur⁴, Sanjit Sahu¹, Tarun Bangia¹, Satheesha S. Poojary², Rajesh B. Jadhav², Shailesh B. Bhat², Ganesh S. Meshram², Harshit Shah², John T. Rayner⁵, Douglas W. Toomey⁶, and Pradeep R. Sandimani²

¹Aryabhata Research Institute of Observational Sciences (ARIES), Manora Peak, Nainital 263 001, India; saurabh@aries.res.in

²Tata Institute of Fundamental Research (TIFR), Homi Bhabha Road, Colaba, Mumbai—400 005, India

³Indian Institute of Astrophysics (IIA), II Block, Koramangala, Bengaluru 560 034, India

⁴Center of Advanced Study, Department of Physics DSB Campus, Kumaun University Nainital, 263001, India

⁵Institute for Astronomy, University of Hawaii, 2680 Woodlawn Drive, Honolulu, HI 96822, USA

⁶Mauna Kea Infrared, LLC, 21 Pookela Street, Hilo, HI 96720, USA

Received 2022 March 22; accepted 2022 July 18; published 2022 August 18

Abstract

We present the design and performance of the TANSPEC, a medium-resolution 0.55–2.5 μm cryogenic spectrometer and imager, now in operation at the 3.6 m Devasthal Optical Telescope (DOT), Nainital, India. The TANSPEC provides three modes of operation, which include photometry with broad- and narrowband filters, spectroscopy with short slits of 20'' length and different widths (from 0''.5 to 4''.0) in cross-dispersed mode at a resolving power R of ~ 2750 , and spectroscopy with long slits of 60'' length and different widths (from 0''.5 to 4''.0) in prism mode at a resolving power R of ~ 100 –350. TANSPEC's imager mode provides a field of view of 60'' \times 60'' with a plate scale of 0''.245 pixel⁻¹ on the 3.6 m DOT. The TANSPEC was successfully commissioned during 2019 April–May, and the subsequent characterization and astronomical observations are presented here. The TANSPEC was made available to the worldwide astronomical community for science observations from 2020 October.

Unified Astronomy Thesaurus concepts: Spectrometers (1554); Direct imaging (387); Near infrared astronomy (1093); Optical observation (1169)

1. Introduction

An instrument with simultaneous optical and near-infrared (NIR) spectroscopic/imaging capabilities on a 4 m class telescope will be an ideal observational tool needed for the efficient usage of telescope time and can act as a workhorse for numerous science cases. Recently, the Aryabhata Research Institute of Observational Sciences (ARIES),⁷ Nainital, India installed a modern 3.6 m new technology optical telescope (3.6 m Devasthal Optical Telescope—DOT⁸), the largest in India, at Devasthal (latitude = 29°21'39".4 N, longitude = 79°41'03".6 E, altitude = 2450 m), Nainital, in Uttarakhand. This facility is a major national observing facility in India, and therefore, it will be of great advantage to complement this telescope with an instrument having simultaneous optical–NIR coverage.

The TIFR-ARIES Near Infrared Spectrometer (TANSPEC) is built in collaboration with the Tata Institute of Fundamental

Research (TIFR),⁹ Mumbai, India; ARIES, Nainital, India; and Maunakea Infrared LLC (MKIR),¹⁰ Hawaii, USA for the 3.6 m DOT. It is a unique spectrograph, providing simultaneous wavelength coverage from ~ 0.55 to 2.5 μm in spectroscopic (cross-dispersed (XD) mode with $R \sim 2750$ and prism mode with $R \sim 100$ –350) as well as in imaging ($r'i'YJHK_s$ bands) modes. The importance of simultaneous optical–NIR observations has been realized in recent years for Galactic and extragalactic astrophysical problems. The TANSPEC will be extremely sensitive to low-temperature stellar photospheres ($T \sim 2500$ K) and objects surrounded by warm dust envelopes or embedded in dust/molecular clouds. It is therefore particularly suited to the study of low- and very-low-mass stellar populations (M/L dwarfs, brown dwarfs), strong mass-losing stars on the asymptotic giant branch (AGB), young stellar objects (YSOs) still in their protostellar envelopes, gravitational lenses, active galactic nuclei, etc. This instrument will also be ideal for producing a spectral library of a large number of stars, which can be used as training samples for future automated stellar classification tools. XD spectroscopy at resolving powers of $R \sim 2750$ (~ 110 km s⁻¹) with a very broad spectral coverage (optical to NIR wavelengths) is very well suited

⁷ <https://aries.res.in/>

⁸ <https://aries.res.in/facilities/astronomical-telescopes/360cm-telescope>



Original content from this work may be used under the terms of the [Creative Commons Attribution 3.0 licence](https://creativecommons.org/licenses/by/3.0/). Any further distribution of this work must maintain attribution to the author(s) and the title of the work, journal citation and DOI.

⁹ <https://www.tifr.res.in>

¹⁰ <http://mkir.com/>

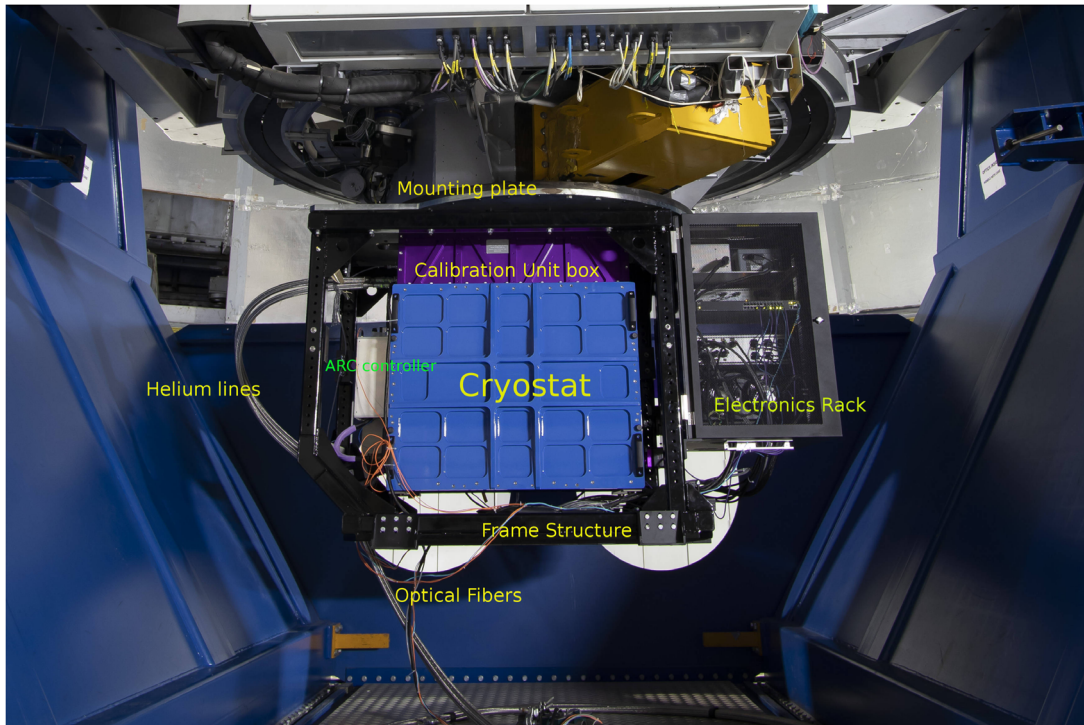


Figure 1. The TANSPEC mounted on the Cassegrain focus of the 3.6 m DOT. Various subcomponents such as the mounting plate, calibration unit box, cryostat, electronics rack, helium lines, frame structure, and optical fibers of the TANSPEC instrument are also shown. The approximate size of this instrument (including the electronic rack and mounting frame) is 2200 mm (length) \times 1100 mm (width) \times 1350 mm (height). The total weight of this instrument is 2000 kg, of which the instrument (blue+purple box) is 650 kg and the mounting plate is 350 kg. The remaining 1000 kg is added to the mounting frame to maintain the center of gravity to balance the telescope.

to identify atomic and molecular features as well as to trace the high-speed dynamics such as stellar winds and broad-lined quasars. Deeply embedded YSOs and molecular species in protostellar disks, comets, and AGB stars are best observed at $\sim 2\text{--}2.5\ \mu\text{m}$. The low-resolution prism mode is optimum for faint-object spectroscopy, such as brown dwarf spectral energy distribution and solid-state features in asteroids and satellites. The long slit in this mode is also useful to study extended objects such as planets and nebulae.

At present, all existing 2 m class telescopes within India (viz. 2.01 m Himalayan Chandra Telescope¹¹ at Hanle, Ladakh; 2 m Inter-University Center for Astronomy and Astrophysics telescope¹² near Pune; 2.34 m Indian Institute of Astrophysics telescope¹³ at Kavalur) have either optical or NIR imager/spectrograph instruments. The TANSPEC is the only instrument in India and one of the few instruments around the globe with simultaneous optical–NIR capabilities. In this paper, we provide the details of the TANSPEC in Section 2 (Overview), Section 3 (Optics), Section 4 (Cryostat), Section 5 (Electronics and Control system), and Section 6 (Software). The details on the detectors and their performance are presented in Section 7. The characterization and performance analyses of the

TANSPEC instrument on the 3.6 m DOT are presented in Section 8, and we conclude in Section 9.

2. Instrument Overview

A photograph of the TANSPEC mounted on the main port (Cassegrain focus) of the 3.6 m DOT through a rigid mounting plate is shown in Figure 1. The cryostat (blue box) is interfaced with a rigid box (purple), which houses a spectral calibration unit consisting of transfer optics, integrating sphere, continuum and arc lamps, and interfaces with the mounting plate of the instrument. The black frame in the photograph is the structure attached to the mounting plate which holds the counterweights to balance this instrument and the electronics rack (black box). The electronics rack holds the power supplies, Ethernet power switches, and temperature controller of the instrument. The photograph also shows the pair of helium lines coming out from the instrument and going through the azimuth axis of the telescope to the ground floor of the telescope building and then to the closed-cycle cryo cooler’s compressor. The optical fibers (orange cables) from the array controllers are going outward to the telescope observing room.

There are three sections that make up the cold optics inside the cryostat: the fore optics, the infrared (IR) slit viewer/guider, and the spectrograph. The initial concept of this instrument is drawn from

¹¹ <https://www.iiap.res.in/?q=iao.htm>

¹² <http://www.iucaa.in/igo.html>

¹³ <https://instru.iucaa.in/index.php/igo>

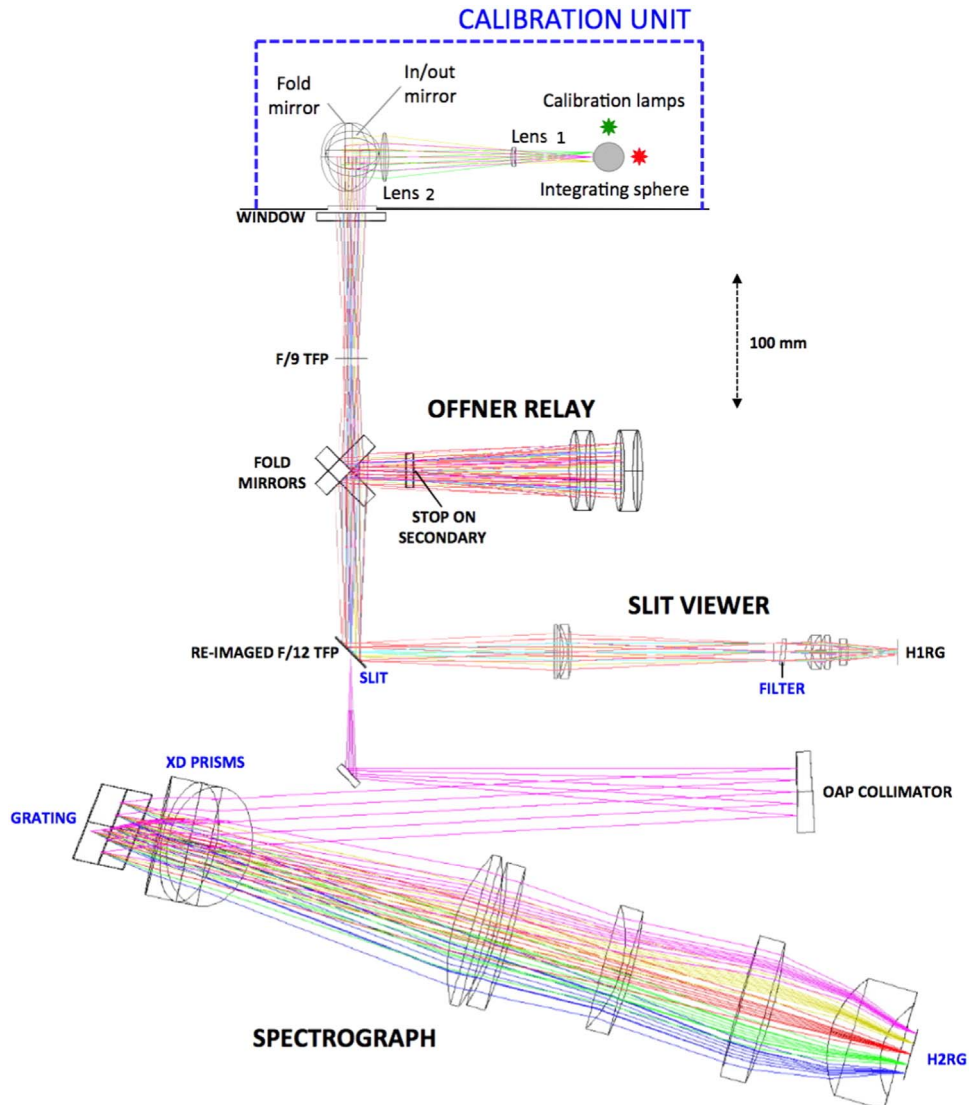


Figure 2. Overall optical layout of the TANSPEC comprising four major components: calibration unit, fore optics (Offner relay), slit viewer, and spectrograph. The $f/9$ beam from the telescope comes to a focus at the telescope focal plane just inside the cryostat window. A 60×60 arcsec² field of view is reimaged by an Offner relay onto the slit where it is reflected into the slit viewer and reimaged onto an H1RG array at $0''.25$ per pixel. A slot in the slit transmits the $f/12$ beam into the spectrograph where it is dispersed and reimaged onto an H2RG array. In this view, ray tracing for order three in the cross-dispersed mode is shown. A warm calibration unit is located above the cryostat window.

the SpeX (Rayner et al. 2003), a medium-resolution $0.8\text{--}5.5\ \mu\text{m}$ spectrograph and imager for the NASA Infrared Telescope Facility (IRTF)¹⁴ in Hawaii. An overall view of the TANSPEC optical layout is shown in Figure 2. Briefly, the $f/9$ beam from the telescope or calibration lamp comes to a focus at the telescope focal plane (TFP) about 100 mm inside the CaF₂ window. The TFP is then reimaged at $f/12$ onto slits in the slit wheel by an Offner relay containing two concave mirrors and one convex secondary mirror. The slit mirrors are tilted at 45° to the incoming $f/12$ beam and reflect it to the slit viewer for imaging and guiding

using the 1024×1024 pixel HAWAII-1RG (H1RG) array. The $f/12$ beam entering the spectrograph through the slot in the slit is first folded and then collimated into dispersing optics. The dispersed beam is focused onto a 2048×2048 pixels HAWAII-2RG (H2RG) array by a set of camera lenses. All the lenses are coated by antireflection in the $0.55\text{--}2.5\ \mu\text{m}$ wavelength range. This was a challenge because the wavelength range is broad and encompasses the visible and NIR range. We were able to achieve designs that gave around 2% reflectivity or less over the full wavelength range. As typical visible wavelength filters are designed for CCDs with a $\sim 1\ \mu\text{m}$ wavelength cutoff, the filter used in the slit viewer is specially designed to block out band

¹⁴ <http://irtfweb.ifa.hawaii.edu/>

wavelengths up to $2.7\ \mu\text{m}$. This is required also because there are much higher background flux levels in the $1\text{--}2.5\ \mu\text{m}$ range. Individual Astronomical Research Cameras (ARC) array controllers run each of the spectrograph and imaging arrays and are mounted on the cryostat. The array controller uses a single-board SPARC computer and four digital signal processor (DSP) boards. A graphical user interface (GUI) of the TANSPEC runs on a Linux workstation placed in the observing room connected to the controllers of the arrays by the optical fibers.

3. Optics

3.1. Calibration Unit

A calibration unit is used for the flat-fielding and the wavelength calibration of the raw spectra taken through this spectrograph. As shown in Figure 2, it has an assembly of calibration lamps, an integrating sphere, camera lenses, and a fold mirror (mounted on a linear translation stage that moves into the telescope beam and picks off the beam from the calibration lamps when required). The pick-off mirror and lamp control can be remotely operated from the instrument software. The calibration optics are designed in a way to match the telescope's f/number and to evenly illuminate the TFP inside the TANSPEC with a 15 mm diameter flat field. This is the size required to cover the longest slits ($60''$). A 12.5 mm diameter exit port (field stop) of an integrating sphere serves as the uniform (Lambertian) flat field. This field is magnified to 15 mm diameter by a 246 mm focal length lens (Lens 1) placed 82 mm from the exit port. A 125 mm focal length CaF₂ lens (Lens 2) reimages this field at 1:1 onto the $f/9$ TFP inside the cryostat. At the same time, Lens 2 images the 15 mm aperture stop of Lens 1 onto the telescope secondary mirror to create an exit pupil identical to that of the telescope so that the calibration light sources illuminate the instrument identically to the telescope. The rms spot diameter in the TFP from the calibration optics is about 0.5 mm. This is sufficient enough to satisfy the uniformity requirement of better than 1% across the slits, which is limited by the integrating sphere. The calibration unit has argon and neon discharge lamps¹⁵ and two tungsten continuum (of different brightness) lamps that cover the entire wavelength range ($0.55\text{--}2.5\ \mu\text{m}$) of the spectrograph.

3.2. Fore Optics

The function of the fore optics is to reimage the TFP onto the slits with the necessary magnification required for the spectrograph. At the same time, an image of the entrance pupil needs to be formed where a cold stop can be located to baffle thermal flux and off-axis scattered light from the telescope. An optimized cold stop cannot be located in the spectrograph because the slit diffractively blurs the entrance pupil image. In the TANSPEC, this is achieved with an Offner relay (see Figure 3), which consists of

three on-axis spherical mirrors. The primary and secondary of the Offner relay consists of two concave and one convex mirror, respectively. The two mirrors of the primary are a little different in focal length so that we can convert from the $f/9$ beam to the $f/12$ beam, which is the desired F-number of the beam at the slit entrance to the spectrograph optics. This results in a slight reduction of the Offner optical performance that is not significant for the system performance. The Offner relay is shown in Figure 3 with the folding flat mirrors removed. It reimages the $f/9$ $60'' \times 60''$ TFP onto the slit plane at $f/12$. We painted the center of the cold secondary of the Offner relay (onto which telescope pupil is imaged) black to work as a cold stop. Being all-reflecting, the Offner relay is completely achromatic and has a high and constant throughput across the desired wavelength range.

3.3. Slit Viewer

The IR slit viewer allows spectra of very red and embedded objects through NIR guiding. It is also a fairly capable imager. The slit viewer is a collimator camera reimaging system consisting of a BaF₂-LiF collimator and LiF-BaF₂-ZnSe camera lenses that reimage the $60'' \times 60''$ slit plane onto the HIRG array with an image scale of $\sim 0''.25$ (see Figure 2). For Nyquist-sampling of the reflected field of view (FOV) of the slit, only the central $480 \times 416\ \text{pixel}^2$ area (starting from $x = 416$ and $y = 288$ pixels) is used. The collimator doublet forms another image of the system entrance pupil where slit-viewing filters are placed (each 25.4 mm diameter). This second stop is not optimized to cold baffle because the cold stop in the fore optics does this. However, it is the best location for the imaging filters (small and uniform pupil image). The slit viewer has a filter wheel with 12 slots to accommodate filters of different wavelengths. This wheel has a position accuracy of $50\ \mu\text{m}$. The details of the filter wheels and filters used in the TANSPEC slit viewer are given in Tables 1 and 2, respectively. The Y , J , H , K_s filters are in the Maunakea Observatory (MKO) system (Tokunaga et al. 2002), made by Asahi Spectra, Japan.¹⁶ The r' , i' , H_2 , and $Br\gamma$ filters are made by Andover Corporation, USA,¹⁷ where the r' , i' filters are in the Sloan digital sky survey (SDSS) system (Bessell 1979). The response curves for all the filters are provided in Figure 4.

3.4. Spectrograph Unit

3.4.1. Slits

The spectrograph unit has a slit wheel with 12 slots to accommodate slits of different sizes and has a position accuracy of $50\ \mu\text{m}$. The details of the slits are listed in Table 1 and are shown in Figure 5. The slits are 1.00 mm-thick fused silica substrates that have an aluminum-coated mirror

¹⁵ <https://www.newport.com/f/pencil-style-calibration-lamps>

¹⁶ <https://www.asahi-spectra.com/>

¹⁷ <https://www.andovercorp.com/>

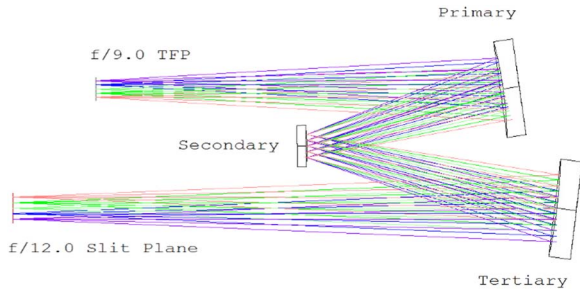


Figure 3. The fore optics reimage the TFP onto the slit plane. This is done with an Offner relay. In this view, the folding mirrors are removed, and the slit plane is shown untilted. The telescope pupil of 14.3 mm diameter is imaged onto the Offner secondary mirror. A cold stop is placed here.

with a slot lithographically applied to the front surface. The slit mirror is oriented at 45° to the incoming $f/12$ beam and reflects a 60×60 arcsec² FOV into the slit viewer. Because the slit is applied lithographically, it is very sharp, and any scatter from the slit edges is minimized. To avoid the ghost reflection at the back surface of the slit substrate entering the spectrograph, an absorbing surface is applied to the back surface of the slit substrate. This back surface has a suitably positioned slot to transmit the primary beam and absorb the ghost. The slit mirrors were coated with aluminum and were made by Photosciences Inc, USA.¹⁸

3.4.2. XD Mode

The $f/12$ beam entering the spectrograph at the slit is first folded and then collimated by an aluminum off-axis-parabolic (OAP) mirror. The OAP and its coatings were done by Durham University, Precision Optics Lab, UK.¹⁹ An image of the entrance pupil (35 mm diameter) is formed at a distance of one focal length from the OAP (420 mm). The grating and prism dispersing elements are located here, housed in the grating wheel. One position of the wheel houses the grating and cross-dispersing double prisms (the XD mode), and the other houses a mirror and single prism (the low-resolution mode). The dispersed beam is focused onto the H2RG array by a five-element refractive camera lens: BaF₂-ZnS-LiF-ZnSe-ZnSe. The optical layout and spectral format of the XD mode are shown in Figure 6. This mode is optimized for wavelengths 0.63–2.54 μm (orders 10–3). To minimize aberrations, these orders are centered on the array and the geometric (untoleranced) resolving power is $R \sim 2750$ at the center of each order. The H2RG array is sensitive from 0.4 to 2.5 μm approximately; therefore, wavelengths 0.63–0.55 μm (orders 11–12) are also imaged onto the array but at slightly reduced resolution due to higher optical aberrations and minor vignetting in the camera lenses.

¹⁸ <https://www.photosciences.com>

¹⁹ <https://dpo.webspace.durham.ac.uk/>

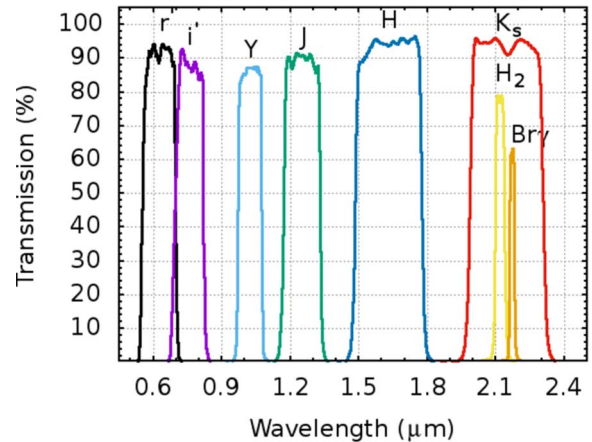


Figure 4. Response curves for the filters used in the slit viewer of TANSPEC.

The configuration for the XD mode of the TANSPEC is given in Table 3. The grating used in the TANSPEC is an off-the-shelf master grating (aluminum substrate) made by Richardson Gratings, USA,²⁰ closely approximating the derived design. Fused silica and ZnSe prisms are used in a double-pass configuration to achieve cross-dispersion over the desired spectral range of ~ 0.55 – 2.5 μm . The prisms are vacuum spaced. There is a slight angle introduced into the second prism so that the two inner surfaces are at an angle to each other. This prevents fringing caused by the two surfaces being parallel. One disadvantage of prisms is that they usually have lower dispersion than gratings. Using the prisms in a double-pass configuration helps to compensate for this. Also, by using prisms made from fused silica and ZnSe, the order separation can be made almost constant in wavelength over the range ~ 0.55 – 2.5 μm leading to much better use of the detector format than is possible for a single prism or grating (order separation is proportional to λ^2).

3.4.3. Prism Mode

In the prism mode, the grating and double prism are replaced by a mirror and single prism (see Figure 7). The prism is made of fused silica and is of a size similar to the cross-dispersing prisms. The prisms and coatings on the prisms were done by Rainbow Research Optics Inc.²¹ The dispersing elements are mounted on a grating wheel. All the other optics are unchanged. Consequently, stray-light levels in the prism mode are very similar to those in the XD mode. The apex of the single fused silica prism is oriented at 90° to the apex of the double prisms of the XD mode so that dispersion is along array rows (in the XD mode, dispersion is along array columns). The resulting dispersion map is also shown in Figure 7. Due to the change in the refractive index of fused silica with wavelength, R changes by a factor of 3 across the wavelength range. The

²⁰ <https://www.newport.com/b/richardson-gratings>

²¹ <https://www.rr-optics.com>

Table 1
The Details of the Filter and Slit Wheels

Position	Filter Wheel		Slit Wheel		
	Filter	Note	Slit Width (")	Slit Length (")	Note
1	<i>J</i>	Broadband filter	0.5	20	XD mode
2	<i>H</i>	Broadband filter	0.75	20	XD mode
3	<i>K_s</i>	Broadband filter	1.0	20	XD mode
4	<i>Y</i>	Broadband filter	1.5	20	XD mode
5	<i>i'</i>	Broadband filter	2.0	20	XD mode
6	<i>r'</i>	Broadband filter	4.0	20	XD mode
7	<i>Brγ</i>	Narrowband filter	0.5	60	Prism mode
8	<i>H₂</i>	Narrowband filter	1.0	60	Prism mode
9	Blank1	...	2.0	60	Prism mode
10	Blank2	...	4.0	60	Prism mode
11	Free slot	...	Mirror	...	Imaging mode
12	Pupil	...	Pupil

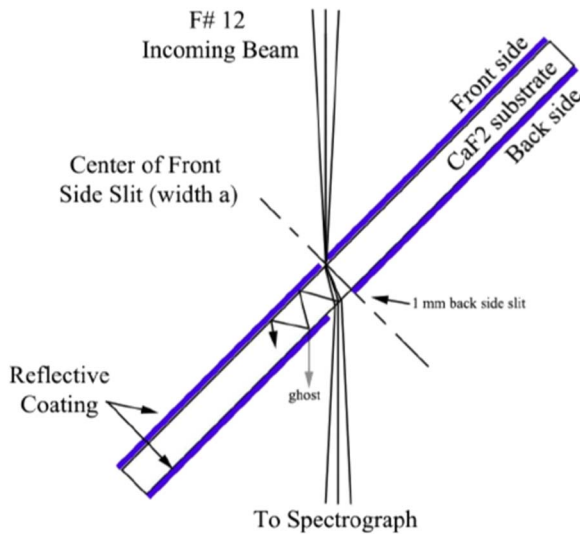


Figure 5. Description of a slit used in the TANSPEC instrument.

prism is designed for $R \sim 100$ matched to the narrowest slit ($0''.5$) at about $1.0 \mu\text{m}$ and is higher at shorter and longer wavelengths. A complication of the design is that the angle required to prevent the input and exit beams to the prism from colliding creates anamorphic shrinking in the dispersion direction. This results in the low-resolution mode $0''.5$ slit being sampled by around three pixels instead of two pixels as in the XD mode (where the anamorphic effects are in the XD direction).

3.4.4. Stray Light and Baffling

A cold stop in the fore optics is used to control the thermal background and stray light from the telescope and sky. The light paths in the instrument are enclosed mostly in baffled

Table 2
Specification of the Filters Used in the Slit Viewer of TANSPEC

Filter Name	Central Wavelength (μm)	Wavelength Range ^a (μm)	Photometric System
<i>r'</i>	0.612	0.555–0.670	SDSS
<i>i'</i>	0.744	0.681–0.805	SDSS
<i>Y</i>	1.020	0.970–1.070	MKO
<i>J</i>	1.250	1.170–1.330	MKO
<i>H</i>	1.635	1.490–1.780	MKO
<i>K_s</i>	2.150	1.990–2.310	MKO
<i>H₂</i>	2.122	2.097–2.138	...
<i>Brγ</i>	2.171	2.160–2.181	...

Note.

^a At 50% transmission of the peak.

tubes in aluminum enclosures. The enclosures are designed in a way to prevent thermal background and stray light from the cryostat components, which are warmer than $\sim 80 \text{ K}$ (e.g., drive shafts, wires, warm vacuum jacket, etc.) that might scatter along the path of the light toward the detectors. The aim of the design was to keep the instrument background below the dark current of the detector ($\sim 0.1 \text{ electron s}^{-1}$). Because of the broad wavelength coverage of the TANSPEC, large variations in either sky or object brightness can occur across the spectra. Therefore, any ghost reflection from the brighter part of the spectrum to the fainter parts can degrade the quality of the data. The main areas of concern are narcissus ghosts from the prisms and camera lens. The ray-tracing of the former suggests that these ghosts can be minimized by tilting the H2RG array by 1° (this is enough to redirect any ghost reflections off the prisms and incur no measurable defocus across the array). The latter are extremely out of focus, but it does not pose any concern. The amount of ghosting in the TANSPEC is of the order of a few percent and can be removed by sky subtraction.

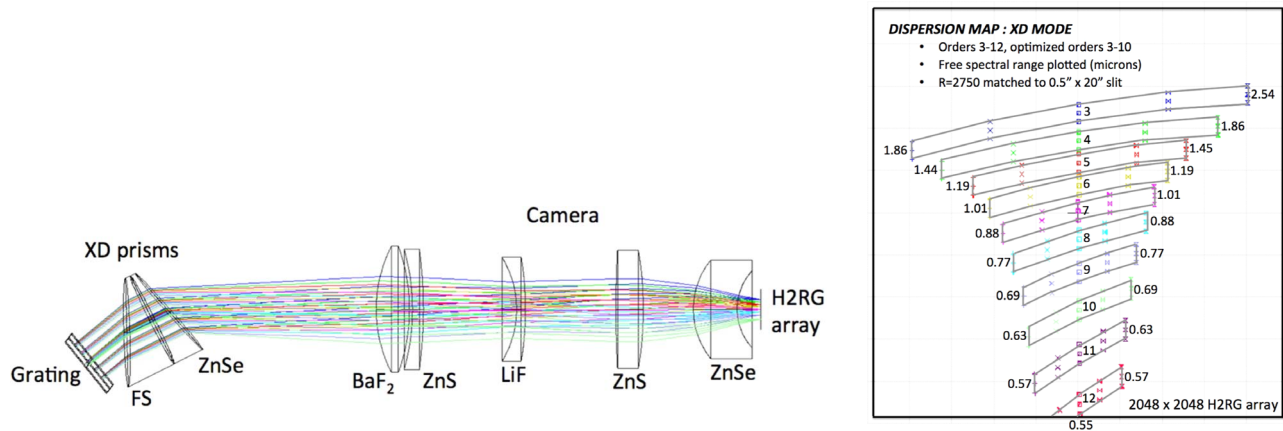


Figure 6. Left panel: ray diagram of the spectrograph XD mode for orders 3–10. Right panel: dispersion map in the XD mode optimized for 2.5–0.63 μm (orders 3–10). Orders 11–12 are covered but with optical aberrations and less sensitivity. The H2RG array is sensitive between $\sim 2.5\text{--}0.4 \mu\text{m}$.

Table 3
TANSPEC Near-Litrow Configuration in the XD Mode

Parameter	Value
R	2750
Slit width	0".5 (2 pixel sampling)
Slit length	20" in XD mode
Collimated beam diameter	35.0 mm
Grating blaze angle	17°5
Grating groove frequency	90 lines/mm
Grating blaze wavelength ($m = 1$)	6.7 μm
Angle between the incident and diffracted beams	9°5
ZnSe prism apex angle	15°
FS prism apex angle	25°
Input beam	$f/12$
OAP focal length	420 mm
OAP off-axis angle	5°5
Camera focal length	144 mm

4. Cryostat

4.1. Mechanical Structure

The entire mechanical assembly of the TANSPEC is shown in Figure 8. The TANSPEC instrument has an envelope size of 1900 mm (width) \times 915 mm (length) \times 1148 mm (height), which is within the telescope instrument envelope. The weight of the TANSPEC and its mounting plate are 650 kg and 350 kg, respectively. Therefore, to balance this instrument and maintain the center of gravity of the 3.6 m DOT, an extra frame with counterweights (1000 kg) on it is added to the instrument. Electronics cabinet containing power supplies, Lakeshore, USA temperature controller²² and Western Telematic Inc. (WTI), USA, Ethernet power switches²³ are also mounted on

²² <https://www.lakeshore.com/products/categories/overview/temperature-products/cryogenic-temperature-controllers/model-336-cryogenic-temperature-controller>

²³ <https://www.wti.com/collections/power-transfer-switch>

this frame. The TANSPEC is attached to the telescope through a mounting plate via a rigid interface box. This box is mounted in between the top plate and the vacuum jacket. A calibration unit is placed inside this box. The box is 280 mm deep, and the walls are of 25 mm thickness. The top plate of the vacuum jacket contains the liquid nitrogen fill port, entrance window, and the mount for the closed-cycle cooler. The TANSPEC along with its frame mounted on the 3.6 m DOT is shown in Figure 1.

The vacuum jacket of the TANSPEC has a four-sided center section weighing about 205 kg and is bolted by two large O-ring sealed covers, each weighing about 38 kg. The four-sided center section is made from four plates of 6061-T6-Aluminum, which are electron-beam-welded together. The vacuum jacket has an external dimension of 1070 mm (length) \times 860 mm (height) \times 630 mm (width). The vacuum jacket has no hard connections except at the rigid top plate (25 mm thick). Therefore, if we can keep the flexures below the yield strength of the aluminum along with the flexure of shafts (connected to the warm motors mounted outside of the vacuum jacket) within the specifications, we can achieve a very stable configuration by using a thick vacuum jacket wall of 25.4 mm, although the large vacuum jacket covers have ribs that taper up to 70 mm. All the internal surfaces are mirror-finished to provide good radiation shielding and to improve the liquid nitrogen (LN₂) hold time. Inside this, there is a radiation shield, which is a closed-cycle cooler-cooled shield that removes most of the thermal radiation from the vacuum jacket. The wall of the LN₂-cooled cold bench/box is 12.5 mm thick and hangs inside the vacuum jacket through fiber-glass V-trusses (3), which are connected to the top plate inside the radiation shield. The detectors are thermally clamped to the cold structure. The radiation shield is mounted around a cold structure through four shear webs connected to the top of the vacuum jacket.

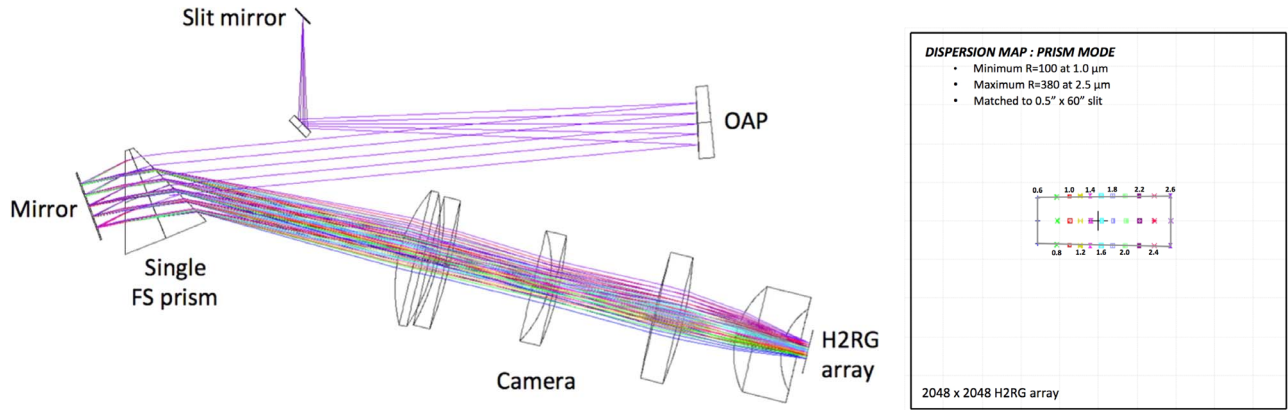


Figure 7. Left panel: ray diagram for the prism (low-resolution) mode. Right panel: dispersion map covering 0.55–2.5 μm wavelength range in the prism mode.

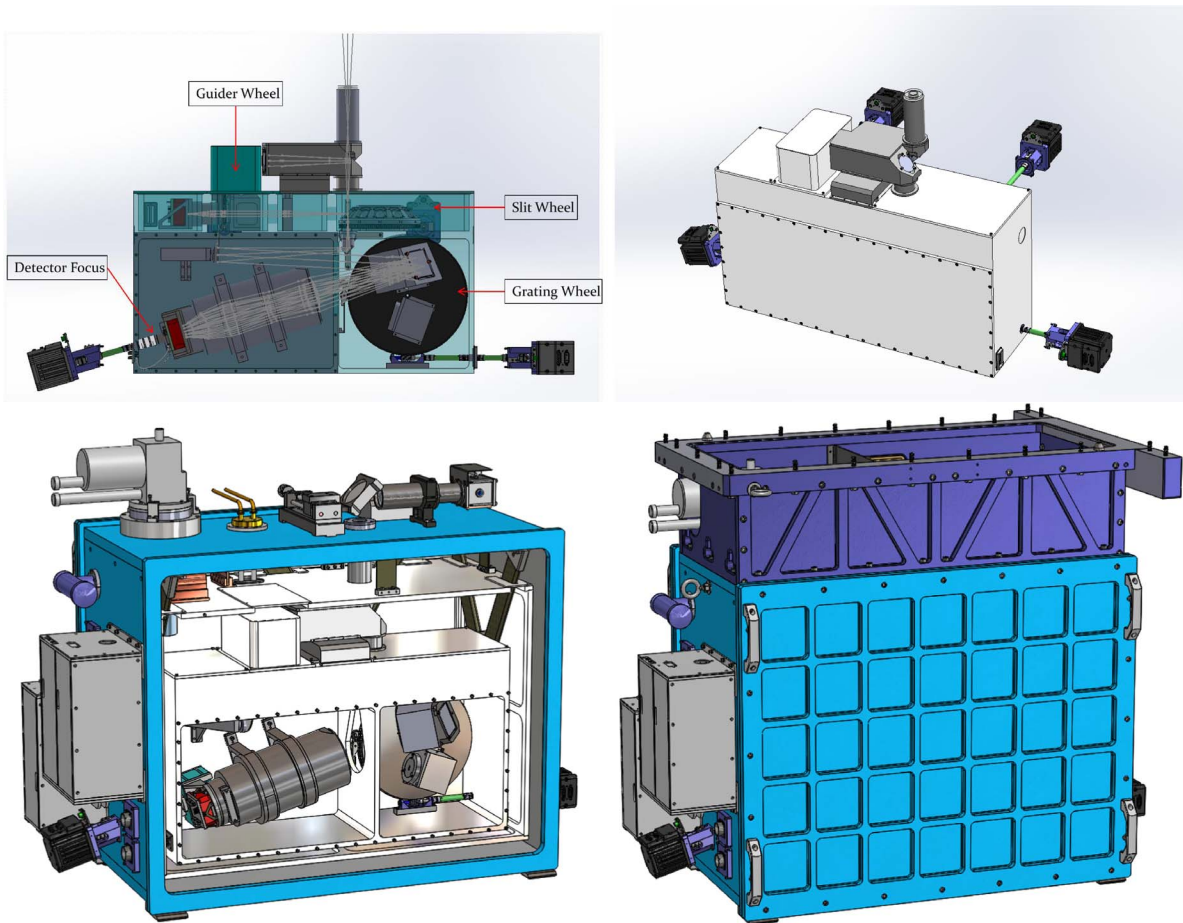


Figure 8. Mechanical assembly of the TANSPEC. The various mechanisms along with the ray trace (top left), cold structure (top right), vacuum jacket (blue box), radiation shield, cold structure along with other components (bottom left), and the entire cryostat assembly (bottom right) along with a top box (purple box containing the calibration unit, LN_2 fill port, cold head) are shown.

4.2. Mechanisms

The TANSPEC has mechanisms for the slit wheel, guide channel filter wheel, grating wheel, spectrograph channel detector focus, and calibration unit pick-off mirror. It uses external warm smart motors manufactured by Animatics Corporation, USA,²⁴ mounted on one of the two covers of the vacuum jacket and coupled to the wheels through ferrofluidic vacuum feedthroughs. The optics and detectors can be accessed by unbolting the opposite covers. There is no need to disassemble motors for the majority of the trouble-shooting inside the cryostat. The array controllers are mounted on the outer surface of the cryostat. The mechanisms have three different categories, i.e., continuously variable wheels, discrete position wheels with detents, and a linear flex stage. For the position sensing, we have used the noncontact Hall effect devices similar to the SpeX instrument (Rayner et al. 1998). All the wheels are equipped with a stationary Hall effect sensor. These sensors are used to encode the wheels' position by placing the magnets at their edges. Opposite polarities signify the homing and other positions. The Hall effect sensor outputs are passed through the comparator circuits and function like limit switches. Stepper motors of 400 steps/revolution in the worm-gear mechanisms are used to drive all the wheels with detented positions, and the final position is determined by counting the steps taken from the home position. The H2RG array focus stage consists of an aluminum alloy flex stage with an antibacklash linear position mechanism that provides ± 2.5 mm of focus travel through a screw coupled with a stepper motor. The calibration lamp assembly has a plane mirror that can be moved by using a motor and linear stage arrangement.

4.3. Cryogenic Design and Performance

The required cooling of this instrument is achieved through a hybrid system with closed-cycle cooling for the radiation shields and LN₂ cooling for the optical bench and detectors. In order to keep the instrument background below the HxRG detector dark current (~ 0.1 electron s⁻¹), LN₂ cooling of the cold structure is done. The radiation shield that surrounds the cold structure is cooled by using a closed-cycle cooler. A cooling temperature of ~ 150 K is sufficient for the radiation shield to reduce the radiation load on the cold structure which can be managed very easily by the LN₂ can. The surface areas of the cold structure, radiation shield, and vacuum jacket are 1.8 m², 2.6 m², and 4.3 m², respectively.

We have used a CTI model 9600 high-voltage compressor²⁵ manufactured by Brooks, USA,²⁶ along with two long (40 m each) pressurized helium lines to cool the highly polished 5 mm thick 6061-aluminum radiation shield to less than 150 K.

The estimated heat load on the cold structure consists of 2.1 W heat from the radiation shield having a temperature of 150 K, 1.9 W from the holes in it (entrance window, etc.), 1.7 W from support V-trusses, 1 W from the wiring, and 0.25 W from the motor shafts. The expected variation in the performance of the closed-cycle cooler does not affect the temperature of the cold structure as its heat load is negligible. The temperature variation due to the boil-off of LN₂ (~ 0.5 K) is also too small to affect the instrument performance (e.g., instrument background or focus).

The instrument can cool down in ~ 60 hr and the hold time for the 14.16 L capacity LN₂ can is ~ 100 hr within an ambient temperature range of 283–301 K. The optical bench and guide detector are maintained at 76 ± 2 K. Warm-up also takes 60 hr, but by bowing out the LN₂ by circulating dry air, the cryostat can be warmed up faster.

5. Electronics and Control System

The overall scheme of the TANSPEC hardware is shown in Figure 9. All instrument electronics along with the instrument are mounted at the telescope Cassegrain port. It consists of the array controllers for the two detectors, preamps, analog-to-digital (A/D) boards, DSP boards, remote Ethernet power control of all elements, mechanism drivers, temperature control monitoring of all parameters, Ethernet switch, power supplies, etc., which are controlled by the Unix Workstations placed in the control room and connected through optical fibers. The wheels, H2RG focus mechanics, and calibration box mirror are moved using independent smart motors. The motors are controlled through a standard Ethernet interface. The electronics cabinet is insulated and designed for glycol cooling to ambient temperature using glycol chillers. The detector arrays are controlled by ARC Gen III controllers (H2RG: four channels and H1RG: one channel) from ARC, Inc., USA.²⁷ It is also known as the Leach Controller or San Diego State University (SDSU) Controller. The configuration of the arrays and their controllers are similar to our previous instrument “TIRSPEC” (see, for details, Ninan et al. 2014). All temperatures (arrays, radiation shield, and cryostat) are monitored using a Lakeshore temperature controller (Model No: 336). The electrical connections and the chassis for the spectrograph controller have provisions to increase the channels to 32 in case the 32 output mode of the H2RG is required at a later stage.

6. Software

The computer in the observing room hosts software to communicate and control individual components such as arrays, mechanism motors, lamps, etc. The software is also interfaced with the Telescope Control System (TCS) and

²⁴ <https://www.animatics.com/>

²⁵ https://www.idealvac.com/files/manuals/Brooks9600High_1.pdf

²⁶ <http://www.brooks.com>

²⁷ <http://www.astro-cam.com/Gen3Products.php>

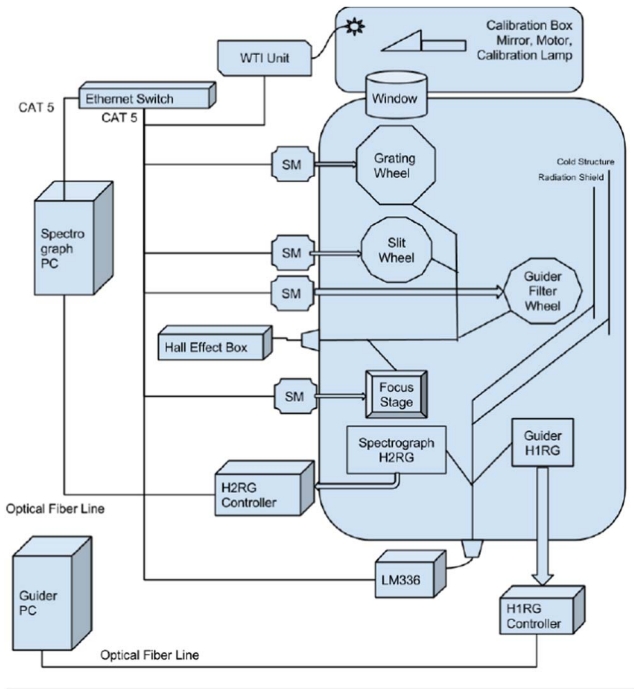


Figure 9. The representative scheme of the TANSPEC Hardware. Apart from a PC (for both guider and spectrograph), all other components are mounted on the telescope either on an electronics rack or on the cryostat of the TANSPEC.

has guiding capabilities. It also fetches header information from the TCS. It has Temperature Control Software for the spectrograph detector and Temperature Monitor Software for the optical bench and Guide Detector. All the mechanisms can be controlled/powered ON through this software along with capabilities to do scripting and macros. In Figure 10, we show the screenshot of the GUI of the TANSPEC, which provides control to the TANSPEC by using various buttons, icons, menus, and macro files.

The overall structure of the TANSPEC software (see also Ninan et al. 2014) is shown in Figure 11. The central server is the command sequencer, and it communicates and controls other servers via UNIX-style sockets. The command sequencer receives the command from the GUI and sends corresponding instructions to other servers (e.g., mechanism server, Array Controller Server (ACS), etc), and then returns instrument status to the GUI. The mechanism server and ACS sends commands to the Animatics Smart-Motor via the Ethernet link and to the ARC controller via the ARC application programming interface (API), respectively. After the data are fully written to the system memory, the PCI board sends an interrupt command to the Central Processing Unit (CPU) and ACS generates a Flexible Image Transport System (FITS) image from the raw data and saves it to the hard disk. It also sends the data via a socket to the quick-look viewer software DV, a data viewer from NASA Infrared Telescope Facility (IRTF),

Hawaii, USA.²⁸ DV has the capabilities to do basic image arithmetic as well as quick measurements to check image quality.

7. Detectors and Their Performance

Two science-grade detectors, H2RG and H1RG, procured from Teledyne, USA,²⁹ are used in the spectrograph and slit viewer, respectively. Their characterization results are provided below.

7.1. Readout Mode and Image Generation

The array is continuously reset pixel by pixel when an exposure is not being taken. When an exposure is requested, the present background reset is completed and then the requested exposure is done. This reduces the after-image and avoids the hard saturating array, and also it sets up a consistent thermal cadence and reduces the thermal anomaly effect. The detector can be read out in various modes, i.e., Single Read, Double Correlated Sampling, and the Sample-Up-The-Ramp (SUTR). The SUTR is the recommended mode of readout as there will be a reduction in the readout noise due to the multiple sampling of the ramp values which reduces the readout noise to about five electrons. The SUTR readout technique is also useful when the pixels are saturated or are hit by cosmic rays (see, for details, Ninan et al. 2014). The flux rate in each pixel is calculated by fitting a line to the counts along the time axis on the SUTR readout data cube. The H2RG array has subarray capabilities in the Y -axis, whereas H1RG has this capability in both the X and Y -axes of the array. There is also built-in software to guide on-slit images and send corrections to the TCS Software to guide on-field objects. In the H2RG array, four vertical strips are read out simultaneously at a rate of $\sim 5 \mu\text{s}$ per pixel, and in total, 5.263 s are required to complete one full-frame read out. Therefore, the exposure time is adjusted automatically to the nearest multiple of 5.263 s (nondestructive readouts of the cumulative counts) and is written to the header of the image file. For the H1RG array, it takes 1.877 s to read out the frame, and therefore, the actual exposure time is adjusted in multiples of 1.877 s. In the top panel of Figure 12, we show the image and distribution of the counts for the first readout of the H2RG array. As H2RG is read out via four channels, we can see four strips for that in the image. A broad intensity distribution with high values as expected in the bias level of NIR detectors is seen. In the lower panel of Figure 12, the same has been shown for the second readout by subtracting the first readout. The sampling clearly shows a Gaussian distribution with a mean around zero and a sigma of ~ 25 Analog to Digital Units (ADU), which is

²⁸ <http://irtfweb.ifa.hawaii.edu/Facility/DV/>

²⁹ <https://www.teledyne.com/en-us>

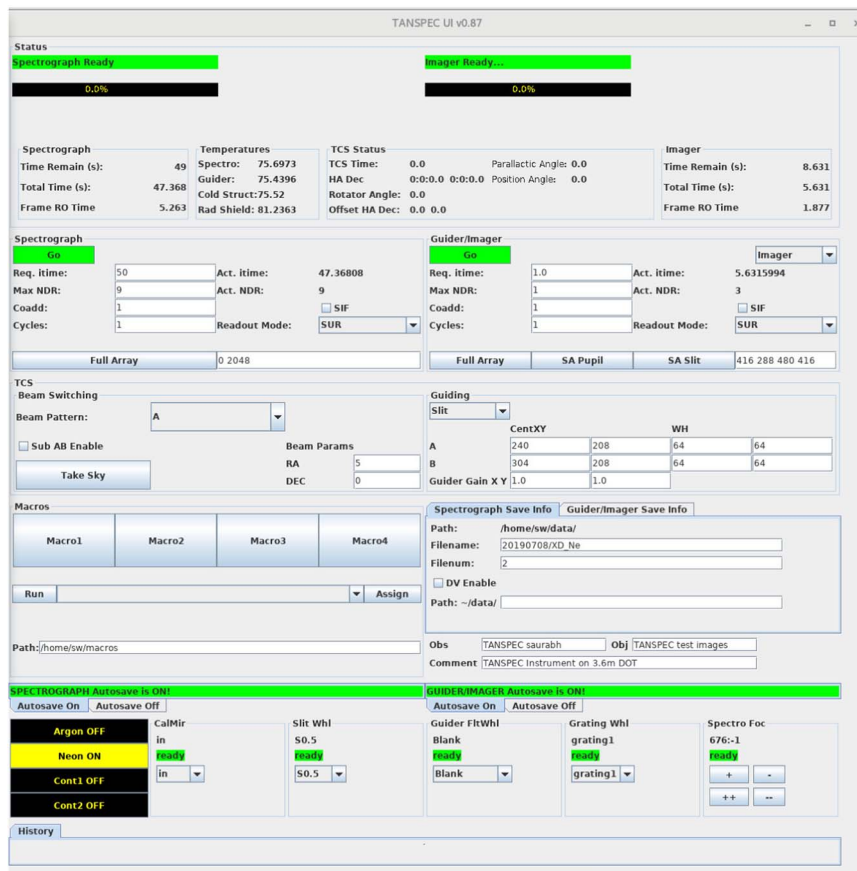


Figure 10. The TANSPEC GUI. It provides control to the TANSPEC by using various buttons, icons, menus, and macro files.

equivalent to the readout noise of the H2RG array in the low-gain setting.

7.2. Gain

We have taken many frames of different exposures with the array exposed to the continuum lamp (for H2RG) and to the telescope enclosure with the $Br\gamma$ filter (for H1RG). Then, for each pixel, we have plotted the counts and their variance (also known as the photon transfer curve) and calculated the slope. The inverse of this slope will be the gain value (see, for details, Ninan et al. 2014). We have selected different regions of box size 5×5 pixels of the exposed area, totaling ~ 500 pixels, of both the H1RG and H2RG arrays for the gain calculation. Figure 13 shows the histograms of the gains obtained for both the H2RG and H1RG arrays. We have fitted a Gaussian function on these distributions and found the peak gain values of $4.5 \pm 0.2 e^-/\text{ADU}$ and $4.3 \pm 0.2 e^-/\text{ADU}$ for the H2RG and H1RG arrays, respectively. In the high-gain setting of the H2RG array, we have found a peak gain value of $\sim 1.12 \pm 0.03 e^-/\text{ADU}$.

7.3. Dark Current

Dark current is estimated by putting a cold block filter in the filter wheel (for H1RG) or the mirror in the slit wheel (for H2RG) and reading out the array. In the left panel of Figure 14, we show the variation of the counts in the dark frame as a function of time for the H2RG (for both high-gain and low-gain settings) and the H1RG arrays. A straight-line fit to this distribution gave a dark current value of $\sim 0.016 \text{ ADU s}^{-1}$ and $\sim 0.013 \text{ ADU s}^{-1}$ for the H2RG (low-gain) and H1RG arrays, respectively. This multiplied by gain values gives us an estimate of the dark current as $\sim 0.07 e^- \text{ s}^{-1}$ and $\sim 0.06 e^- \text{ s}^{-1}$. Similarly, in the high-gain setting of the H2RG array, the dark current is $\sim 0.07 e^- \text{ s}^{-1}$. A few sets of dark-frame readouts at the beginning and end of each night would be enough for its correction.

7.4. Readout Noise

Because the dark current is very small, for the readout noise calculation, we have used a set of frames generated from the difference of consecutive frames of a dark exposure. We have calculated the standard deviation in the count values for each

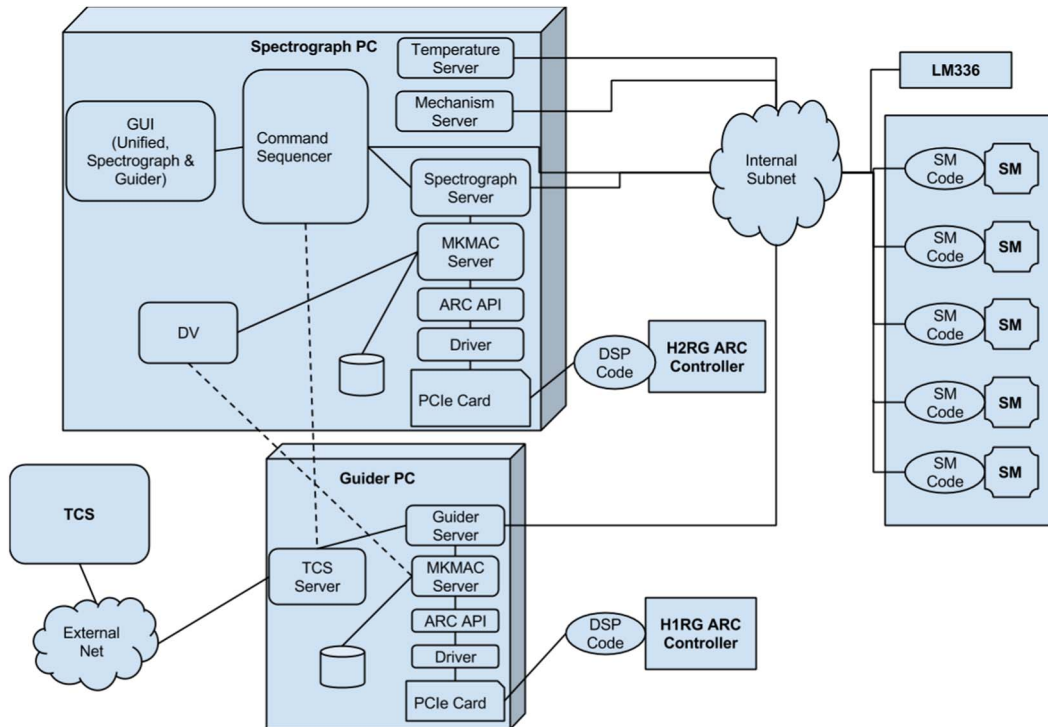


Figure 11. A representative scheme of the TANSPEC software. A PC (both for spectrograph and slit viewer/guider) is placed in the observing room with different servers, PCI cards, and software. The PC is also connected with TCS (for its feedback/control), array controllers, different mechanisms, etc.

pixel in the above set of frames. This standard deviation is actually $\sqrt{2}$ times the readout noise value of each pixel (see, for details, Ninan et al. 2014). The distribution of the readout noise for all pixels in the arrays is shown in the right panel of Figure 14. The readout noise for the H2RG (low-gain) and H1RG arrays is found to be 5.3 ± 0.7 and 3.5 ± 0.1 ADUs, respectively. In the high-gain setting of the H2RG, the readout noise is estimated as 20.7 ± 3.5 ADUs. Here, it is worthwhile to mention that the above readout noise values are for a single readout. The readout noise is a function of the number of readouts and will decrease with an increase in the number of readouts, e.g., in the case of H2RG, the readout noise will be 1.2 ADUs for 284 readouts (or $5.3 e^-$, low-gain setting). For more details, please see Wilson et al. (2019).

7.5. Linear Range and Saturation Levels

Using the SUTR readout data of the continuum lamps (for H2RG array) and argon lamp with the $\text{Br}\gamma$ filter (for H1RG), we have estimated the median saturation level of these arrays as $\sim 28,000$ ADU ($\sim 65,000$ ADU for high gain) and $\sim 32,000$ ADU, respectively, for the low-gain setting. In Figure 15, we show the variation of the median intensity value as a function of exposure time for these arrays for the low-gain setting. We can clearly see the saturation levels along with the nonlinearity in the curves near these limits. We have estimated the median

value of the upper limit for the linear regime of the H2RG and H1RG arrays as 26,000 ADU (57,000 ADU for high gain) and 30,000 ADU, respectively. As the median bias level for the H2RG and H1RG arrays are at $\sim 20,000$ ADU (20,000 ADU for high gain) and $\sim 13,000$ ADU, the effective (useful) well depths for these arrays are found to be at the level of ~ 6000 ADU ($\sim 37,000$ ADU for high gain) and $\sim 17,000$ ADU, respectively, in the low-gain setting. Here, it is worthwhile to mention that very bright spectral lines or stars can result in residual images that can contaminate the darks.

7.6. Bad, Hot, and Cold Pixels

The pixels that deviate more than 8σ from the median value in the image generated by dividing two flats (taken in low and high incident flux) are defined as bad pixels. The percentage of the bad pixels in the H1RG array is 0.03%, most of which are along the edges. For the H2RG array, which is used for spectroscopy, the different orders observed in continuum lamps were used to detect bad pixels, which are negligible in number.

The pixels having counts more than 8σ above the median value in a dark readout of 100 s are defined as hot pixels. The fraction of hot pixels for the H1RG and H2RG arrays was found to be 0.05% and 0.03%, respectively. They are distributed randomly over the arrays. Similarly, cold pixels (pixels that have counts less than 8σ below median value in a

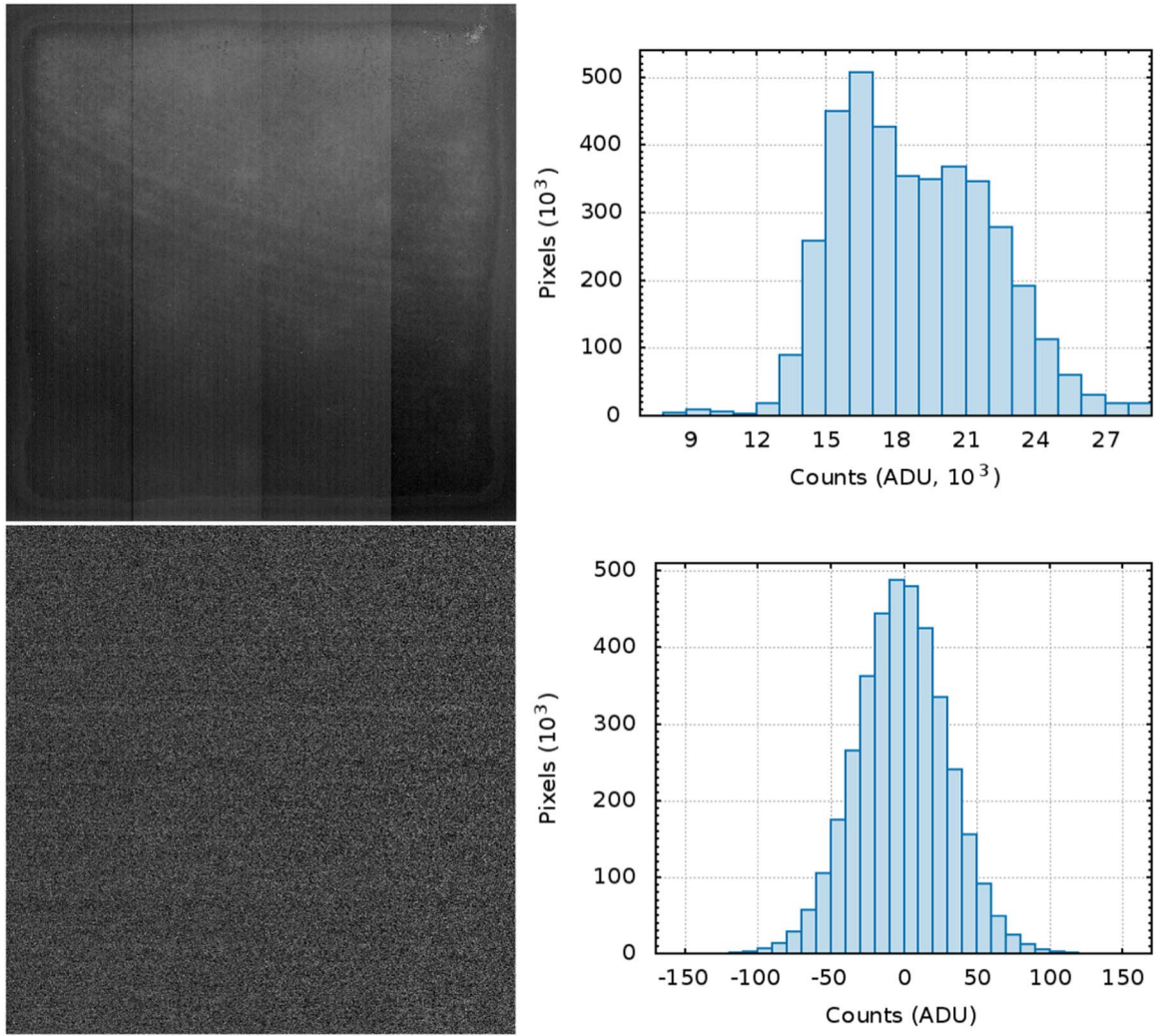


Figure 12. Upper panels: image and histogram of the first readout (bias level) of the dark image for the H2RG array in the high-gain setting. Lower panels: similar to the above but for the second readout after subtracting the first readout.

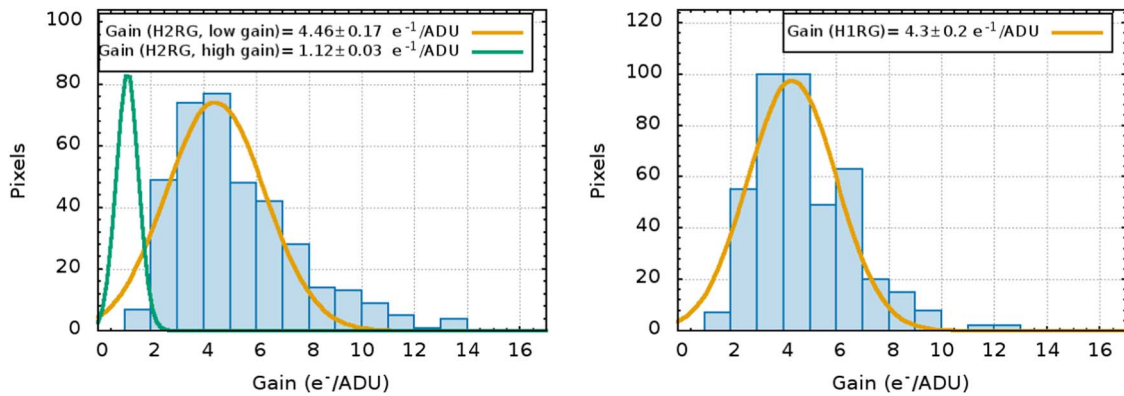


Figure 13. Distribution of gain values for the H2RG array in low/high-gain settings (left panel) and for the H1RG array (right panel). The thick line is a Gaussian fitted curve on the distribution.

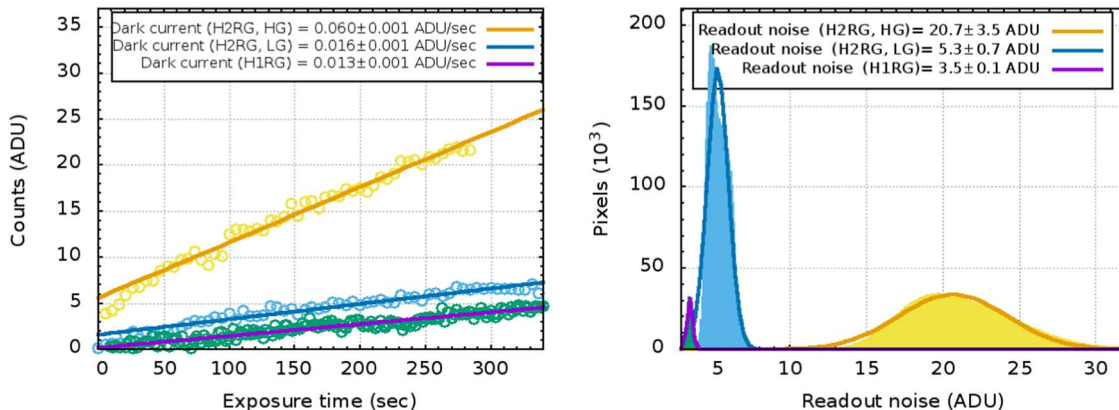


Figure 14. Dark current (left panel) and readout noise (right panel) for the H2RG array in both high-gain (HG) and low-gain (LG) settings and for the H1RG array.

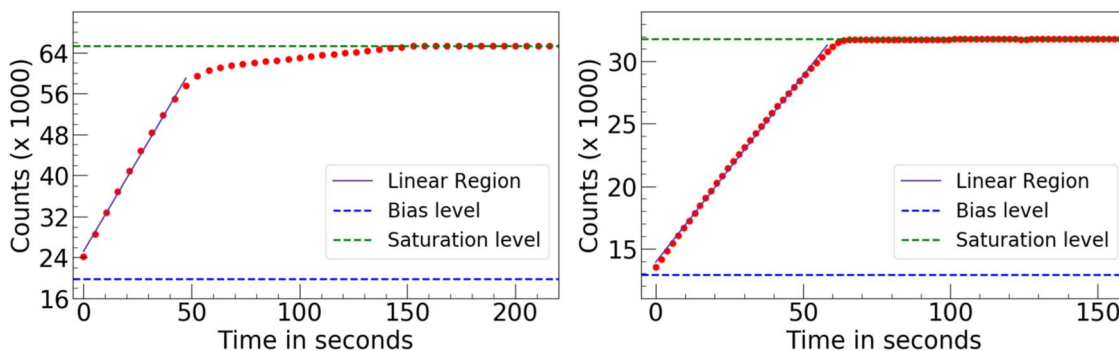


Figure 15. Linear range and the saturation values for the H2RG (left panel) and H1RG (right panel) arrays.

dark readout of 100 s) fraction was found to be negligible for both arrays.

The main parameters of the H2RG and H1RG arrays used in the TANSPEC instrument are listed in Table 4.

8. Performance on the 3.6 m DOT

Ground testing of the TANSPEC was carried out during the first week of 2019 April, and subsequently, it was mounted on the 3.6 m DOT. The TANSPEC was then used for on-sky commissioning tests during 2019 April–May. We present initial results in the following subsections.

8.1. Observing Procedure

The detailed procedure for observing through the TANSPEC is provided in the TANSPEC observation manual.³⁰ Briefly, the observer selects the required slit and spectroscopy mode (XD mode or prism mode) through the slit wheel and grating wheel, respectively. The desired filter can be selected through the filter

wheel, and the target source is then imaged in the slit viewer/guider. Afterwards, the target source is placed in the center of the slit by giving offsets to the telescope. Guiding can also be done with the slit viewer through any filter (optical to NIR) on an object in its FOV. The magnitude limit for autoguiding is roughly about $J \sim 10$ mag in an exposure of 10 s. The telescope's visible guider can also be used to guide stars. Once guiding is started, a long integration of several hundred seconds can be done on the faint sources. In order to correct the spectra for the sky lines, telluric standards should be observed near the target source at about a similar airmass. Calibration frames such as arc lamps, dark, and flats are usually taken at the standard star position by executing a calibration macro. All updates and information about the TANSPEC instrument are provided on the ARIES 3.6 m DOT instrument page.³¹ The initial version of the data reduction pipeline, pyTANSPEC,³² which supports the XD mode data reduction for slits of width $0''.5$ and $1''.0$, is also released.

³⁰ <https://aries.res.in/sites/default/files/files/3.6-DOT/Tanspec-Observation-Manual.pdf>

³¹ <https://aries.res.in/facilities/astronomical-telescopes/360cm-telescope/Instruments>

³² <https://github.com/astrosupriyo/pyTANSPEC>

Table 4
Main Parameters of the Detectors Used in the TANSPEC Instrument

Parameter	H2RG (High Gain)	H2RG (Low Gain)	H1RG
Number of pixels	2048 × 2048	2048 × 2048	1024 × 1024
Pixel size (μm)	18	18	18
Gain (e^-/ADU)	1.1	4.5	4.3
Readout noise (ADU)	20.7 ± 3.5	5.3 ± 0.7	3.5 ± 0.1
Dark current (ADU/sec)	0.060 ± 0.001	0.016 ± 0.001	0.013 ± 0.001
Saturation (ADU)	65,000	28,000	32,000
Use full-well depth (ADU)	37,000	6000	17,000
Readout time (sec)	5.263	5.263	1.877
Readout channels	4	4	1
Sampling	Single read, Up the Ramp, Double Correlated Sampling, Nondestructive Reads (NDRs)	same	same
Subarray capability	In the Y-axis	In the Y-axis	In both the X- and Y-axes

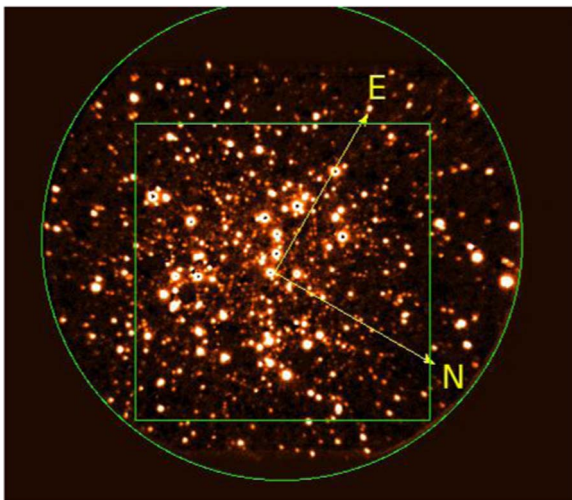


Figure 16. Image of the globular cluster M53 taken in the K_s band using the slit viewer of the TANSPEC on 3.6 m DOT on 2019 April 20. The subarray of the H1RG array is used to image a circular FOV of sky having a radius of $49''$ (shown as a green circle) through a mirror in the slit wheel and a filter in the filter wheel. The image quality of the FOV is optimized for the $60'' \times 60''$ FOV (shown as a green box). The FOV of the slit viewer is rotated by 120° in the clockwise direction, which can be aligned by offsetting the rotator of the telescope by 120° .

8.2. Imaging: Slit Viewer

By using the slit viewer in the TANSPEC mounted on the 3.6 m DOT, we can image celestial objects on the H1RG array.

8.2.1. Field-of-view, Plate Scale, and Image Quality

An image of the globular cluster M53 taken in the K_s band using the slit viewer of the TANSPEC on 3.6 m DOT is shown in Figure 16. The subarray of the H1RG array is used to image a circular FOV of sky having a radius of $49''$ (shown as a green circle in Figure 16) through a mirror in the slit wheel and a filter in the filter wheel. The image quality is optimized for the $60'' \times 60''$ FOV (please refer to Figure 16). Astrometry of the image of the astronomical objects obtained by using the slit viewer was done by

using the Graphical Astronomy and Image Analysis Tool³³ with an rms noise of the order of $\sim 0''.25$. The plate scale was estimated as $0''.245 \text{ pixel}^{-1}$. The FOV of the slit viewer is rotated by 120° in the clockwise direction, which can be aligned in the celestial north-south direction by offsetting the rotator of the telescope by 120° .

An example of typical stellar profiles in K_s and r' bands using the slit viewer on the TANSPEC is shown in Figure 17. We have observed several regions in photometric nights to check for the variation of the FWHM in different directions. The size (FWHM) of the point-spread function (PSF) of the stellar images is found to be around $\sim 0''.45\text{--}0''.60$ in the K_s band ($2.2 \mu\text{m}$) and $\sim 0''.6\text{--}0''.7$ in the r' band ($0.61 \mu\text{m}$). This is in accordance with the wavelength dependence of the atmospheric seeing.³⁴ The images are also found to be circular in shape (ellipticity = 0.02–0.2). There is no direction-dependent variation in the PSF of the stellar images.

8.2.2. Color Equations

We took NIR observations of a field near the W51 star-forming complex ($\alpha_{2000} = 19^{\text{h}}25^{\text{m}}40^{\text{s}}$, $\delta_{2000} = +15^\circ 07' 46''$) with four frames of 10 s exposure in a five-point dither pattern in J , H , and K_s filters. We also did an observation of the open cluster Be 20 ($\alpha_{2000} = 05^{\text{h}}32^{\text{m}}36^{\text{s}}$, $\delta_{2000} = +00^\circ 11' 19''$) in the optical r' and i' bands with 12 frames of 5 minute exposures, i.e., a total of 1 hr exposure in the r' and i' filters. Dark frames and sky flats were also taken during the observations. The sky frames in the NIR filters (JHK_s) were generated by median-combining the dithered frames. The basic image processing such as dark/sky subtraction and flat-fielding was done using tasks available within the Image Reduction and Analysis Facility (IRAF).³⁵ Instrumental magnitudes were obtained using the DAOPHOT package. As the target region was crowded, we carried out the PSF photometry to get

³³ <http://star-www.dur.ac.uk/~pdraper/gaia/gaia.html>

³⁴ https://www.astro.auth.gr/~seeing-gr/seeing_gr_files/theory/node17.html

³⁵ IRAF is distributed by the National Optical Astronomy Observatory, which is operated by the Association of Universities for Research in Astronomy (AURA) under cooperative agreement with the National Science Foundation.

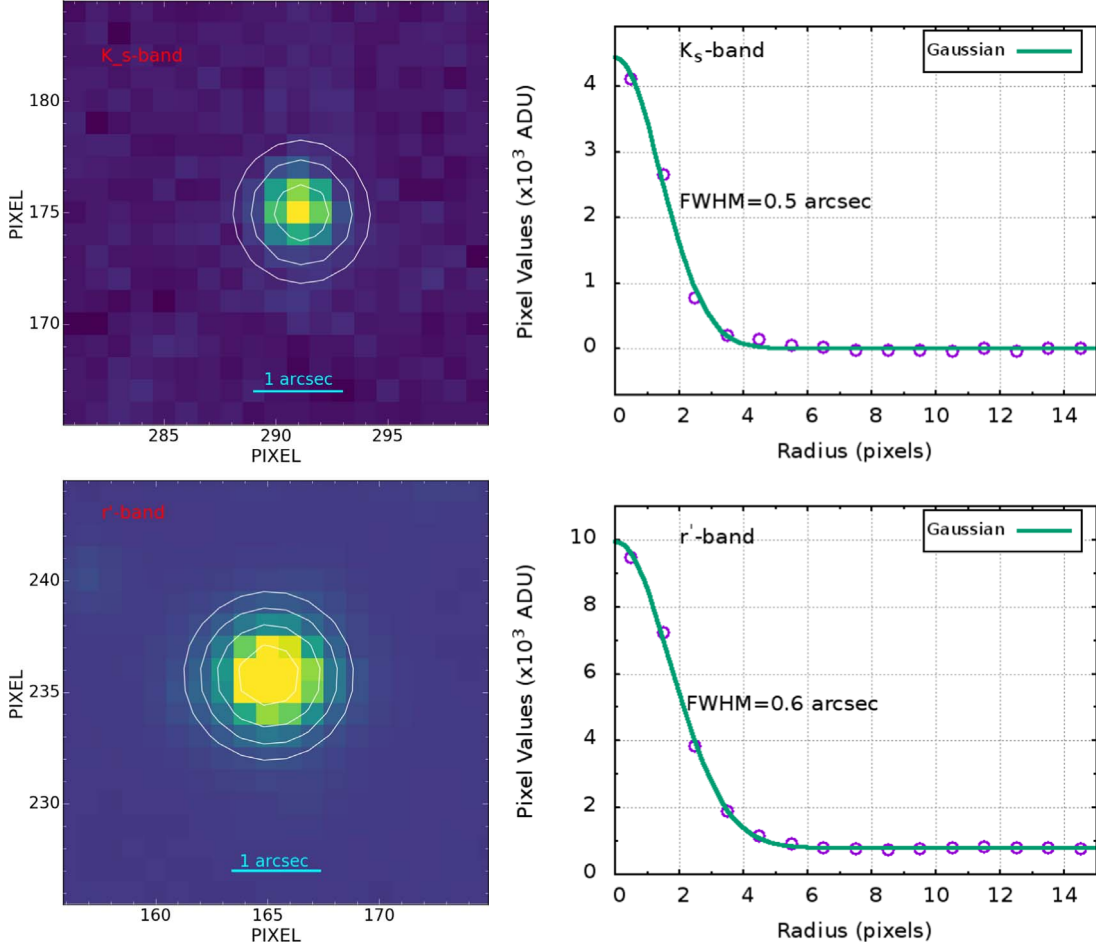


Figure 17. Shape and radial profile of stars in the K_s (upper panels) and r' (lower panels) bands using the slit viewer on the TANSPEC. The FWHM of the stellar profile is $0''.5$ and $0''.6$ in the K_s and r' bands, respectively.

the magnitudes of the stars. The obtained color correction equations for the NIR filters (JHK_s) of the TANSPEC on the 3.6 m DOT for calibrating to Two Micron All Sky Survey (2MASS) magnitudes are as follows (see also Ghosh et al. 2022):

$$(J - H) = (0.91 \pm 0.07) \times (j - h) + 0.05 \pm 0.08 \quad (1)$$

$$(H - K) = (1.01 \pm 0.07) \times (h - k) + 0.51 \pm 0.05 \quad (2)$$

$$(J - K) = (1.17 \pm 0.05) \times (j - k) - 0.70 \pm 0.12 \quad (3)$$

$$(J - j) = (0.004 \pm 0.04) \times (J - H) - 1.21 \pm 0.04 \quad (4)$$

where JHK are the standard magnitudes of the stars taken from the 2MASS catalog (Cutri et al. 2003) and jhk are the present instrumental magnitudes of the same stars normalized per second of exposure time.

The color correction equations obtained for optical filters (r' and i') of the TANSPEC on the 3.6 m DOT for calibrating to the Panoramic Survey Telescope and Rapid Response System (Pan-STARRS1 or PS1 Chambers et al. (2016)) are obtained as follows:

$$(r_{P1} - i_{P1}) = (0.99 \pm 0.03) \times (r - i) - 0.06 \pm 0.01 \quad (5)$$

$$(r_{P1} - r) = (0.08 \pm 0.06) \times (r_{P1} - i_{P1}) - 6.14 \pm 0.02 \quad (6)$$

$$(i_{P1} - i) = (-0.01 \pm 0.01) \times (r_{P1} - i_{P1}) - 6.05 \pm 0.02 \quad (7)$$

where r_{P1} and i_{P1} denote the standard magnitudes of the stars taken from the PS1 data release 1 catalog,³⁶ and r and i are the present instrumental magnitudes of the similar stars normalized per second of exposure time.

8.2.3. Sensitivity

To estimate the photometric sensitivity, we took deep NIR observations of the open cluster Teutsch 76 ($\alpha_{2000} = 22^{\text{h}}28^{\text{m}}47^{\text{s}}$, $\delta_{2000} = +61^{\circ}37'55''$) with five frames of 20 s exposure in a seven-point dither pattern in the J , H , and K_s filters. We took five sets of these observations, which give a total exposure time of ~ 1 hr in the J , H , and K_s filters. For optical bands, we have used the deep data of the open cluster Be 20 with an hour exposure each in r' and i' filters, as

³⁶ <http://catalogs.mast.stsci.edu/>

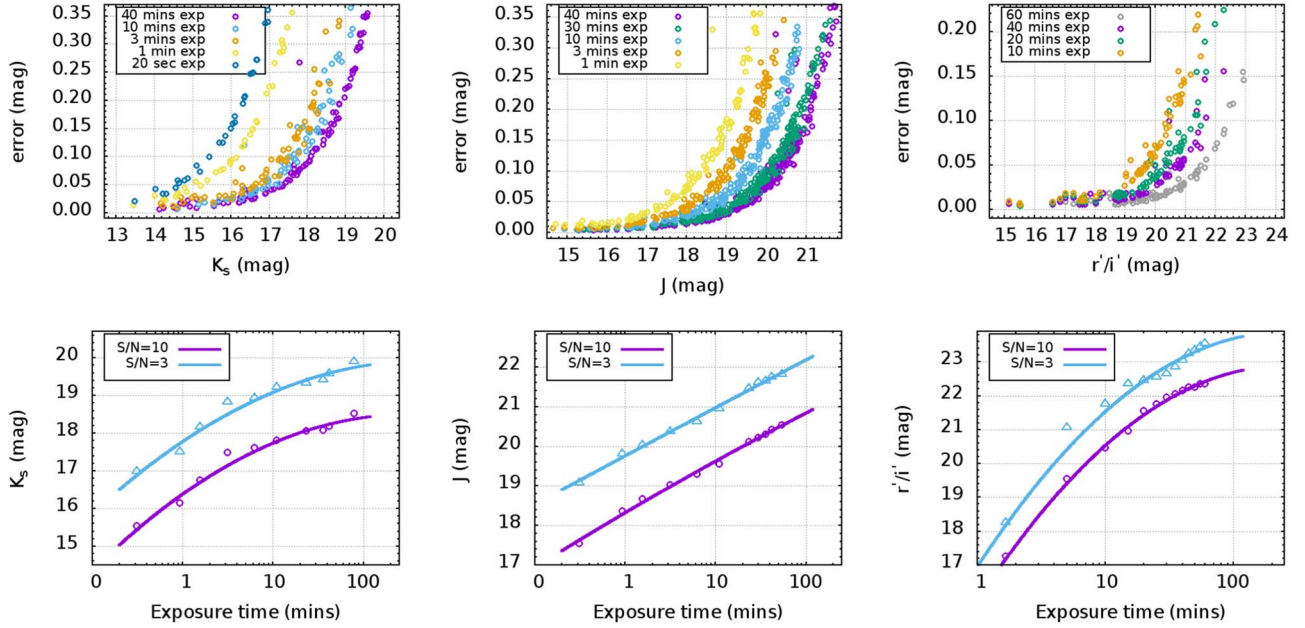


Figure 18. Sensitivity curves for the slit viewer in the TANSPEC instrument. Top panels: error as a function of magnitude in the K_s , J , and r'/i' bands for different exposure times. Bottom panels: K_s , J , and r'/i' magnitudes as a function of exposure time for $S/N = 10$ and 3 . The solid curves are the fitted function on the data points shown by open circles/triangles.

discussed in the previous section. Individual cleaned images were average-combined to give the final image on which we have done photometry as per the procedure mentioned in the previous section. The FWHMs of the stellar profile in these final images were around $\sim 0''.8$ (NIR bands) and $\sim 1''$ (optical bands), respectively. The observations were carried out at an approximate elevation of 55° – 45° . The humidity was around 40%–60%, and the temperature ranges from 4° to 12° Celsius.

The top panel of Figure 18 shows the magnitude versus error plot for different exposures for the stars in the cluster field in the IR and optical filters. Using these plots, we have generated the exposure time versus magnitude graphs in different filters for signal-to-noise ratio (S/N) = 10 and $S/N = 3$ (detection limit), which are shown in the bottom panels of Figure 18. The curved lines are the polynomials fitted to the data points generated by the smoothed spline function on the observed data points. These curves are generated with an M1 reflectivity value of 90%. Clearly, the TANSPEC has a sensitivity to detect a faint source of $K_s \sim 19.7$ mag or $r' \sim 23.7$ (with an S/N of 3) in 2 hr of exposure. An exposure-time calculator based on these curves is under development.

8.3. Spectroscopy: XD Mode and Prism Mode

8.3.1. Wavelength Range

The calibration unit of the TANSPEC has argon and neon lamps for wavelength calibration and two continuum lamps for flat-fielding the spectra taken in both XD and prism modes. The argon lamp covers mostly the NIR part of the spectra whereas the neon lamp covers mostly the optical part. Two continuum

lamps, one at high voltage and another at low voltage, are used to cover all the orders of the spectra. The aperture on the integrating sphere is fine-tuned in such a way that the spectra do not get saturated in both modes of the TANSPEC.

In the top panels of Figure 19, we show the images of the Neon lamp (left panel) and the stellar spectra of the Wolf–Rayet (WR) star “HD 16523” (right panel) in the XD mode of the TANSPEC. These images were taken with a $0''.5$ slit having a $20''$ length. Exposure times for argon/neon lamps and a WR star ($K \sim 7.9$ mag) were 120/100 s and 450 s, respectively. All the orders starting from 3rd (1.86 – $2.54 \mu\text{m}$) to 12th (0.55 – $0.57 \mu\text{m}$) are detected in both the lamps and stellar spectra. The spectra of a WR star clearly show the broad emission-line features in almost all orders. The sky lines and thermal background at longer wavelengths ($\lambda \gtrsim 2.3 \mu\text{m}$) are also seen in the stellar spectra. The sky lines are mostly OH emission and can be subtracted using the spectra of a telluric standard. The thermal background can be due to several reasons, e.g., thermal emission from the telescope and dome structure, and can add noise in that part of the spectra. As can be seen from the images, all orders in the lamp spectra have sufficient lines that can be used to wavelength-calibrate the stellar spectra. The lower panel of Figure 19 shows the extracted wavelength-calibrated spectra for both lamps (left panel) and star (right panel) for all the orders. They also show the good coverage of lines required for wavelength calibration as well as various spectral features of a WR star. Wavelength calibration was done using the IDENTIFY task in IRAF with an accuracy of $0.1 \mu\text{m}$, and the reciprocal linear dispersion was ~ 1 – 4 \AA pixel^{-1} .

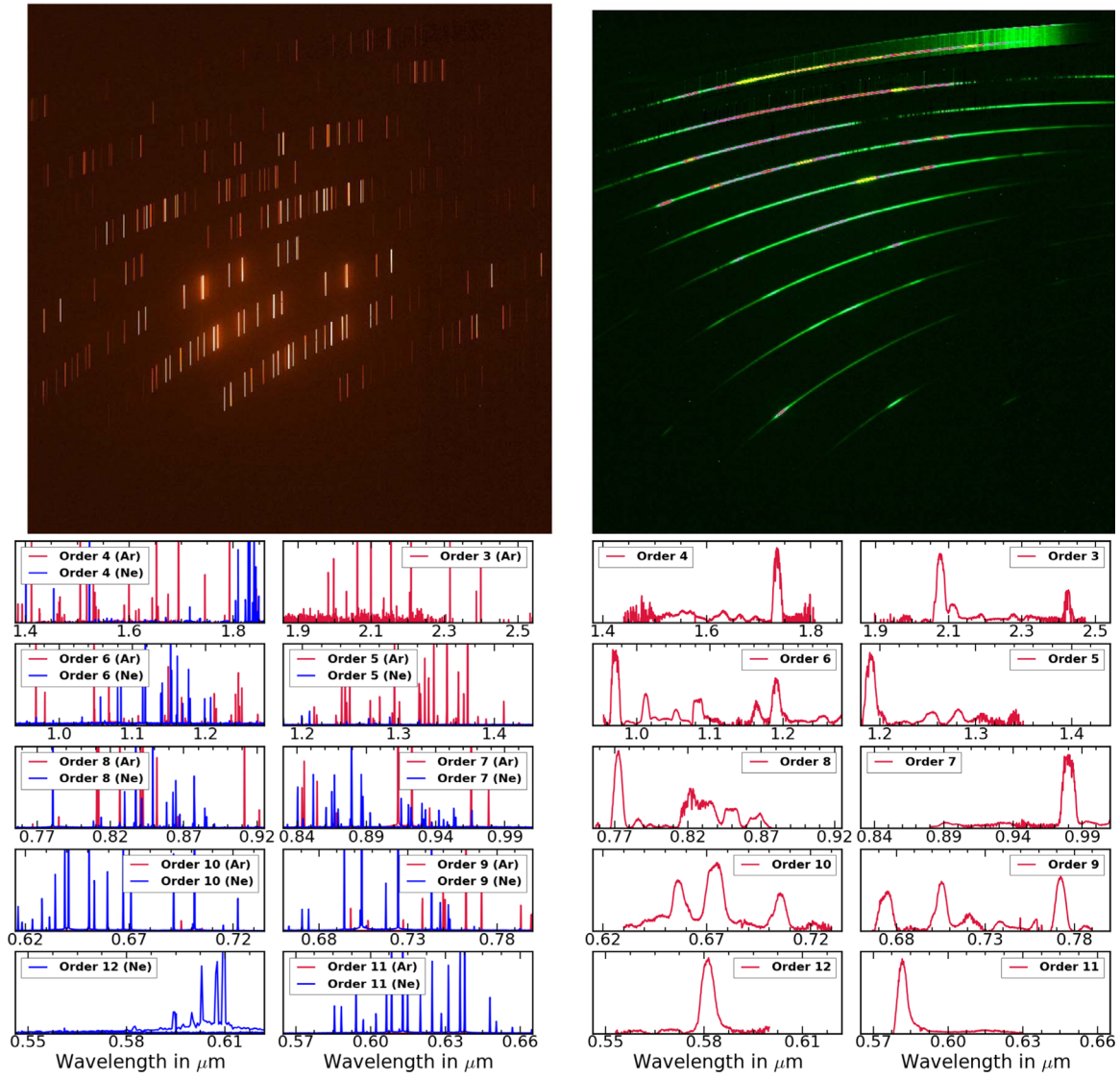


Figure 19. Images of the neon lamp spectra (top left) and the spectra of the WR star “HD 16523” (top right) taken through the TANSPEC in XD mode. The wavelength-calibrated spectra in different orders of the XD mode of the TANSPEC for neon/argon lamps (bottom left) and a WR star (bottom right).

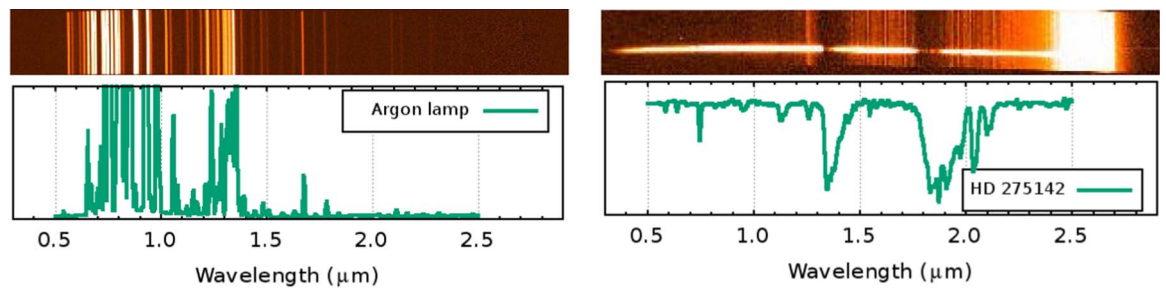


Figure 20. Images of the argon lamp spectra (top left) and F-type star “HD 275142” spectra (top right) taken through the TANSPEC in the prism mode. The wavelength-calibrated spectra in the prism mode of the TANSPEC for the argon lamp (bottom left) and “HD 275142” star (bottom right).

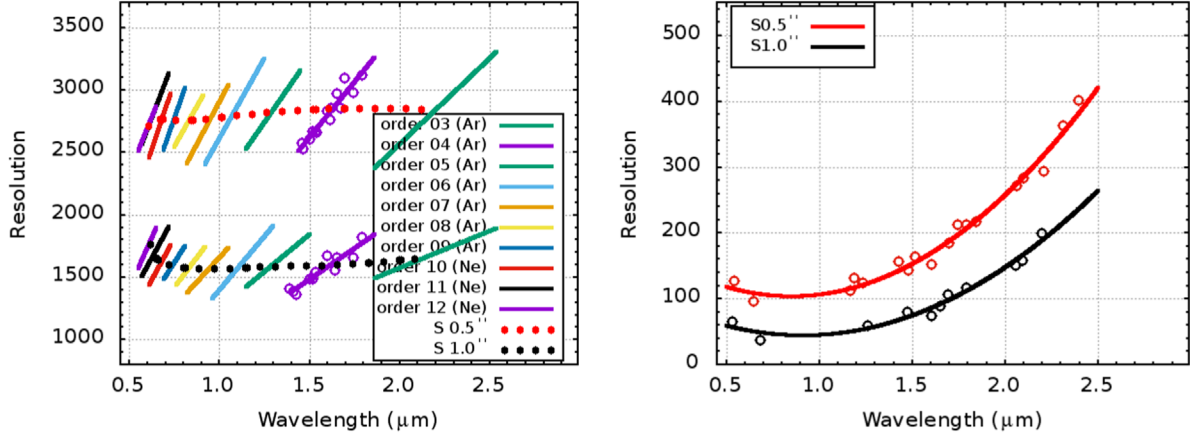


Figure 21. Spectral resolution as a function of wavelength in the XD mode (for different orders, left panel) and the prism mode (right panel) of the TANSPEC for the $0''.5$ and $1''$ wide slits. The solid curves are fitted functions on the data points shown as open circles (for clarity, we have shown data points only for the fourth order in the XD mode).

Table 5

Estimate of the Throughput (in %) of the TANSPEC Instrument for Best Optics Performance Including the Telescope Mirrors, Instrument Mirrors/Lens/Prism/Grating/Substrate and the Quantum Efficiencies of the Detector Arrays at Different Wavelengths

Bands (μm)	$r'(0.66)$	$i'(0.81)$	Z(0.9)	Y(1.02)	J(1.22)	H(1.63)	$K_s(2.19)$
Imaging mode	42	40	51	55	58	60	63
XD mode	22	20	26	28	29	31	33
Prism mode	37	33	42	45	48	52	36

Similarly, in the top panels of Figure 20, we show the images of the neon lamp (left panel) and stellar spectra of the F-type star “HD 275142” (right panel) in the prism mode of the TANSPEC. These images were also taken using the $0''.5$ slit having a $20''$ length. Exposure times for the argon/neon lamps and HD 275142 ($K \sim 9.7$ mag) were 3.5 s and 150 s, respectively. The lower panel of Figure 20 shows the extracted wavelength-calibrated spectra for both lamps (left panel) and star (right panel) in the prism mode. From Figures 19 and 20, we can also see the full wavelength coverage of the instrument from 0.55 to $2.5 \mu\text{m}$. Sky lines and thermal background are also evident in the spectra. No stellar features are seen at some wavelength regimes because of the atmospheric absorption due to H_2O and OH bands. Wavelength calibration was done with an accuracy of $0.4 \mu\text{m}$, and the reciprocal linear dispersion was $\sim 1\text{--}4 \text{ \AA pixel}^{-1}$.

8.3.2. Spectral Resolution

The effective spectral resolving power of the spectra in each order was estimated by finding the FWHMs of the argon/neon lamp lines through slits of $0''.5$ and $1''.0$ widths. Figure 21 shows the spectral resolving power ($\lambda/\Delta\lambda$) as a function of wavelength for the $0''.5$ and $1''.0$ slits as obtained from the argon/neon lines in the XD mode (left panel) and the prism mode (right panel) of the TANSPEC. The median resolution in the XD mode is estimated as 2750 and 1600 for $0''.5$ and $1''.0$

slits, respectively. For the prism mode, the resolution varies from $100''$ (50) to $400''$ (250) for the $0''.5$ (1.0) slit across different regions of the spectra, respectively.

8.4. Throughput

For an efficient throughput, the entire optics needed to work efficiently across the entire $0.55\text{--}2.5 \mu\text{m}$ range of the instrument. The theoretical estimates of the throughput of the TANSPEC instrument in different modes at different wavelengths are given in Table 5. These numbers are estimated for the best optics performance of the system, including the telescope mirrors, instrument mirrors/lens/prism/grating/substrate, and quantum efficiencies of the arrays at different wavelengths. However, these estimates can be treated as upper limits as they do not include the atmospheric transmission and the slit losses. As expected, there is a decrease in throughput at shorter wavelengths (r' and i' bands) due to the combination of decreasing quantum efficiency (QE) of the array (including its own single-layer antireflection coating) and decreasing efficiency of the broadband antireflection (BBAR) coatings on the transmissive optics. The peak throughput of the XD mode is about $\sim 30\%$. On the other hand, the peak throughput of the prism mode ($\sim 50\%$) is far more than that of the XD mode. The imaging mode peak throughput is estimated as $\sim 60\%$.

The throughput of the entire system in the imaging mode was also measured from the total flux of standard stars in an

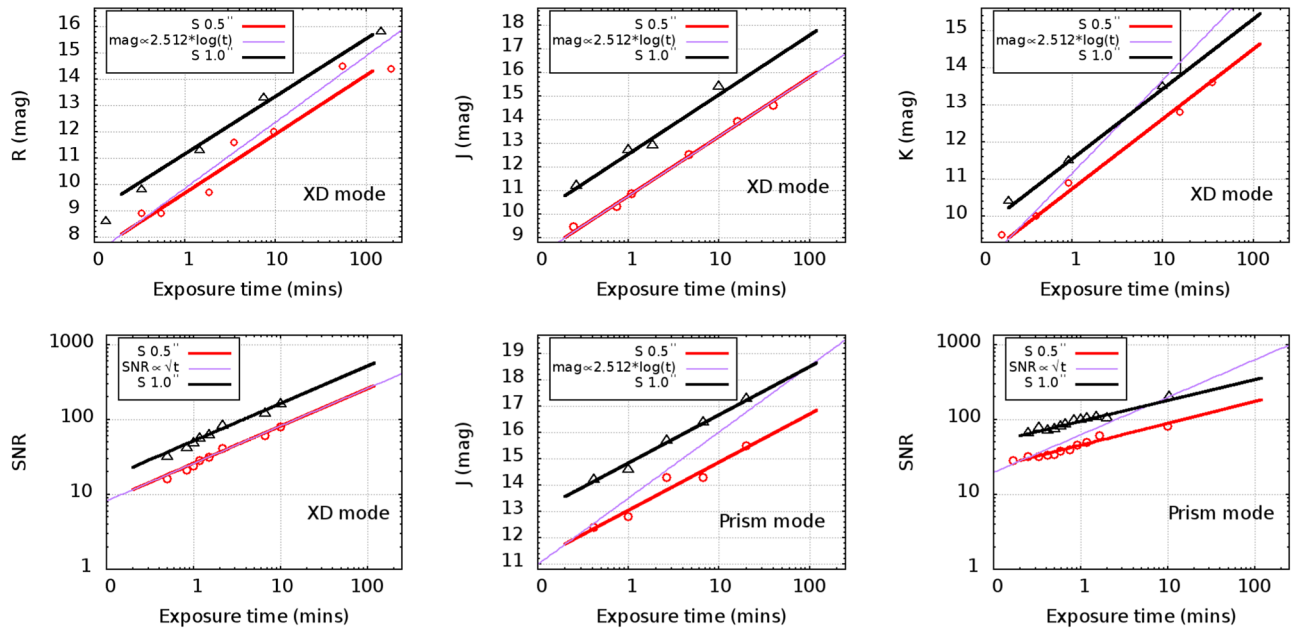


Figure 22. Sensitivity curves for the spectroscopic mode of the TANSPEC on the 3.6 m DOT. Thick lines are the magnitudes (for $S/N = 10$) and S/N vs. exposure-time curves for the XD mode and the prism mode of the TANSPEC for both $0.5''$ (red color) and $1.0''$ (black color) wide slits. Magenta lines are the scaling relationships ($S/N \propto \sqrt{t}$, $\text{mag} \propto 2.512 \cdot \log(t)$) normalized at short exposure time for the $0.5''$ slit. The thick curves are the fitted function on the data points shown by open circles/triangles.

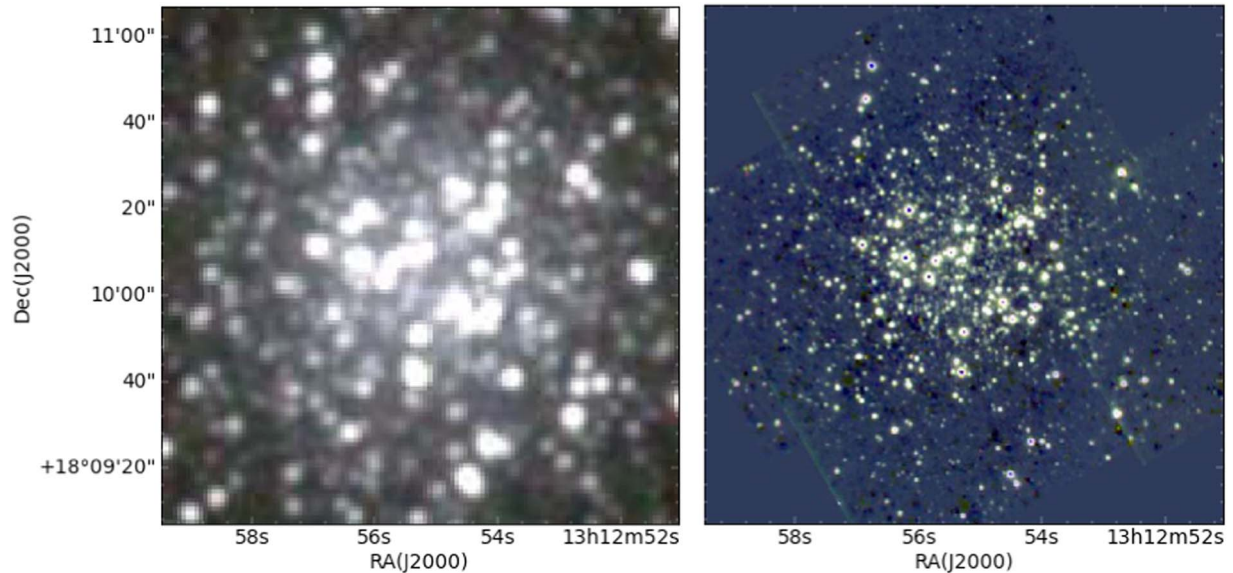


Figure 23. Comparison of the color-composite images of the $\sim 2' \times 2'$ FOV of the central region of the M53 globular star cluster generated by using the K_s - (red), H - (green), and J -band (blue) images from 2MASS (left panel) and TANSPEC (right panel).

area of 4 times the FWHM of their profile. The imaging mode throughput percentage is $30\% \pm 5\%$, $45\% \pm 5\%$, $44\% \pm 5\%$, and $35\% \pm 5\%$ for the r' , J , H , and K_s bands, respectively. The lower K_s -band throughput may be due to the higher background at these wavelengths, i.e., thermal background and atmospheric lines. These numbers also include other parameters such as the QE of

the detector, instrument/telescope optics, and the atmospheric turbulences. The throughput in spectroscopy mode is very difficult to measure as it involves placing the star at the exact center of the slit every time. However, the throughput in the prism and XD modes was measured on an A0V star through a $1''$ wide slit. We used the J -band region of the spectrum to calculate the throughput.

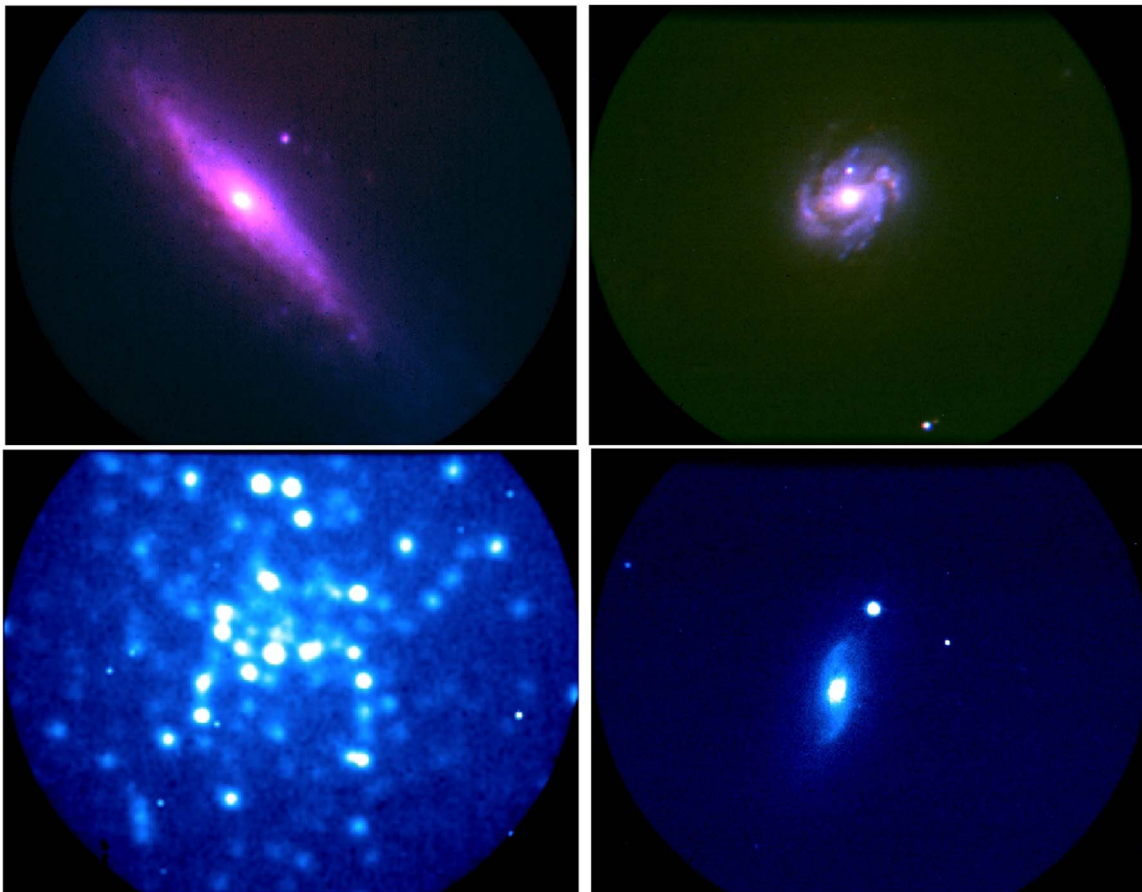


Figure 24. Color-composite images of galaxies NGC 4666 (top-left) and NGC 4328 (top-right) using J (blue), H (green), and K_s (red) images taken through the slit viewer of the TANSPEC. J -band images of the globular star cluster “Palomar 2” (bottom left) and the Seyfert galaxy “MCG+09-16-013” (bottom right) are also shown.

The theoretical J -band flux for the star was calculated using Pogson’s relation³⁷ where the zero-point of the magnitude is taken from the literature (Cohen et al. 2003). This value was converted to photon counts by dividing it with the energy corresponding to the J -band wavelength. The observed photon counts were converted to units of counts/m²/s by dividing them by the effective collecting area and the total integration time. The ratio of the observed values to the theoretical values is obtained as 21% and 37%, which are the throughput values of the spectrograph in the XD and prism modes, respectively. As expected, the measured throughput values are lower than the theoretical estimates due to the atmospheric transmission and the current reflectivity of the primary mirror of the 3.6 m DOT, i.e., 45%–60% in optical bands. Slit losses can also contribute to the low throughput values, and a wider slit, e.g., 4”, can help minimize those losses.

8.4.1. Sensitivity

Sensitivity in spectroscopic mode is estimated by taking the spectra of A0V stars having a range of magnitudes. During

³⁷ $M = 2.512 \cdot \log(F) + C$

observations, the stellar FWHM, relative humidity, temperature, and reflectivity of the M1 mirror of the 3.6 m DOT were 0”6–1”0, <60%, 5°–15° C, and ~50%, respectively. Figure 22 shows various estimates of the exposure time required for a continuum S/N of 10 in different bands/orders of the XD mode as well as for the prism mode of the TANSPEC for the 0”5 and 1”0 wide slits. The S/N is quite sensitive to the FWHM of the star profile as well as the accuracy in the centering of the star inside the slit. Therefore, the 1”0 slit provides better sensitivity than the 0”5 slit. We have found that the spectra of stars up to 15 mag (K_s), 17.5 mag (J), and 15.5 mag (R) can be observed in 2 hr of exposure with a 1”0 slit (with an S/N of 10) under typical night conditions. The S/N is also calculated from the extracted spectra of a $J = 10$ mag A0V star in 0”5 and 1”0 slits and its variation with exposure time is also plotted in Figure 22 for the XD and prism modes of the TANSPEC. Deviation of the S/N from the \sqrt{t} line is possible when there are other sources of noise contributing on top of the photon noise. This can happen when counts are less, and the read noise is comparable to photon noise. The S/Ns at NIR bands are also prone to high background noises (thermal, atmospheric lines, etc.) and can contribute to this deviation.

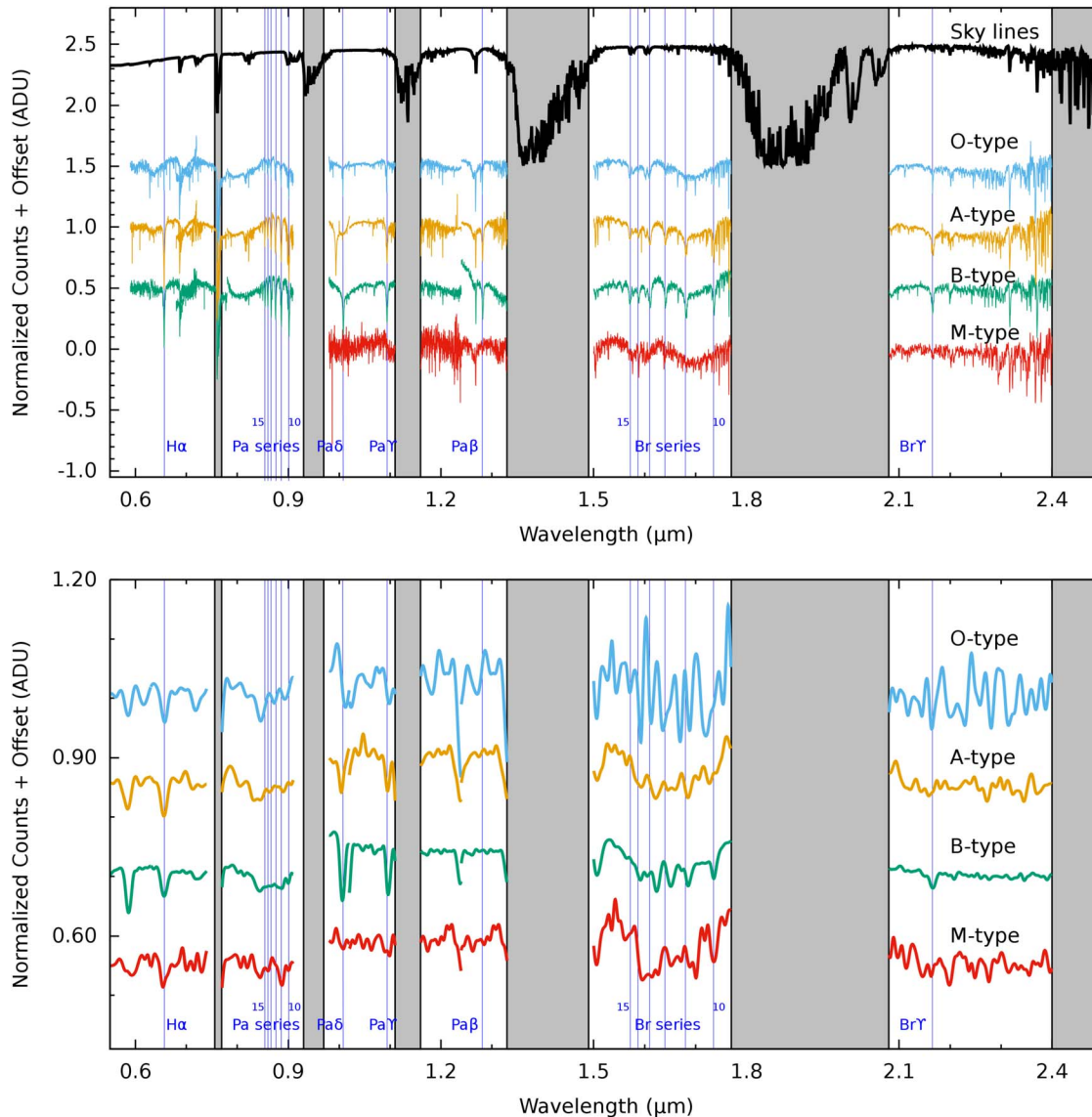


Figure 25. Sample spectra of stars of different spectral types in the XD mode (top panel) and the prism mode (bottom panel) of the TANSPEC taken with a $0''.5$ slit. The shaded regions are the regions where atmospheric features dominate. Various detected spectral lines are also marked.

8.5. Example Images and Spectra

During the commissioning nights of the TANSPEC instrument, we have observed various astrophysical sources in the spectroscopy as well as imaging modes. We have done observations of the M53 globular cluster using the slit viewer in the TANSPEC on the 3.6 m DOT. As the FOV of the slit viewer is small ($\sim 60'' \times 60''$), we have done observations of M53 in five pointings in the J -, H -, and K_s -band filters with 25 nondestructive reads (NDRs). The readout time of each NDR is 1.877 sections. In Figure 23, we show the comparison of the mosaicked image of the slit viewer with that of the 2MASS survey. We can easily see a better resolved and deeper image

from the TANSPEC. Figure 24 shows color-composite images created from the J , H , and K_s images and J -band images of some of the sources observed with the TANSPEC. Figure 25 shows the optical–NIR spectra obtained from stars with different spectral types in both the XD and prism modes of the TANSPEC. The black curve is the atmospheric transmission at Maunakea.³⁸ The shaded regions are thus the regions where atmospheric features dominate the spectra, and hence, we have not shown those wavelength ranges in our extracted

³⁸ <http://twiki.cis.rit.edu/twiki/bin/view/Main/MaunaKeaTo100kmAtmosphericTransmissions>

Table 6
Main Parameters of the TANSPEC Instrument

Parameter	XD Mode	Prism Mode	Imaging
Wavelength Coverage (μm)	0.55–2.5	0.55–2.5	0.55–2.5
Resolution ^a ($\frac{\lambda}{\Delta\lambda}$)	2750	~100–350	~10
Plate scale (arcsec/pixel)	0.25	0.25	0.25
Throughput (% at the J band)	30	48	58
Sensitivity ^b (mag)			
i'	15.7	17.0	22.5/ 20.5/16.0 ^c
i'	15.7	17.0	22.5/20.5/16.0
J	17.7	19.0	20.5/19.7/18.4
H	16.0	17.3	19.5/18.7/17.4
K_s	15.7	17.0	18.3/17.7/16.4

Notes.

^a For the $0''5$ slit.

^b For 90% telescope reflectivity, 1 hr exposure, $1''0$ slit, $1''$ seeing, and $S/N = 10$.

^c 1 hr/10 minute/1 minute exposure.

spectra. We can easily identify various spectral features (marked as blue vertical lines) in both spectra.

9. Conclusion

The TANSPEC is a unique instrument that has the ability to deliver a simultaneous optical–NIR ($0.55\text{--}2.5\ \mu\text{m}$) spectrum in a single exposure. The TANSPEC was delivered and commissioned on the 3.6 m DOT successfully. It has been used for both commissioning tests and science observations during 2019–2020. The two spectroscopic modes of the TANSPEC, XD mode and prism mode, provide spectra with resolutions $R \sim 2750$ and $R \sim 100\text{--}350$, respectively. The main parameters of the TANSPEC obtained during commissioning tests and science observations are tabulated in Table 6. It was officially released to the astronomy community in 2020 October and is currently being used heavily for science observations by many astronomers worldwide.

We thank the anonymous reviewer for valuable comments, which greatly improved the content of the paper. We thank the staff of the 3.6 m DOT and 1.3 m DFOT, Devasthal (ARIES), for their cooperation during the observations. It is a pleasure to thank the members of the IR astronomy group (Department of Astronomy and Astrophysics) at TIFR for their support during observations. We acknowledge the Spex instrument,³⁹ which we relied heavily on for the initial concept and the many practical lessons learned from that instrument. The Project In charge (PI) and Co-PI of the TANSPEC project are thankful to the funding agencies (Department of Science and Technology (DST) and Department of Atomic Energy (DAE), Government of India, India) for approving the project and the Directors of TIFR and ARIES for their support and encouragement. Thanks to the ARIES Governing council and Project Management Board (PMB) (3.6 m DOT) for reviewing from time to time the progress of the project, and finally, the DOT and TIFR teams for their support during the installation and commissioning of the TANSPEC on 3.6 m DOT. Finally, the TIFR team acknowledges the support of the DAE, Government of India, under project Identification No. RTI 4002. The authors would like to thank Dr. Brijesh Kumar (Astronomer In-charge, 3.6 m DOT) for his support during the commissioning of TANSPEC on the 3.6 m DOT.

ORCID iDs

Saurabh Sharma  <https://orcid.org/0000-0001-5731-3057>

References

- Bessell, M. S. 1979, *PASP*, **91**, 589
 Chambers, K. C., Magnier, E. A., Metcalfe, N., et al. 2016, arXiv:1612.05560
 Cohen, M., Wheaton, W. A., & Megeath, S. T. 2003, *AJ*, **126**, 1090
 Cutri, R. M., Skrutskie, M. F., van Dyk, S., et al. 2003, *yCat*, **2246**, 0
 Ghosh, A., Sharma, S., Ninan, J. P., et al. 2022, *ApJ*, **926**, 68
 Ninan, J. P., Ojha, D. K., Ghosh, S. K., et al. 2014, *JAI*, **3**, 1450006
 Rayner, J. T., Toomey, D. W., Onaka, P. M., et al. 1998, *Proc. SPIE*, **3354**, 468
 Rayner, J. T., Toomey, D. W., Onaka, P. M., et al. 2003, *PASP*, **115**, 362
 Tokunaga, A. T., Simons, D. A., & Vacca, W. D. 2002, *PASP*, **114**, 180
 Wilson, J. C., Hearty, F. R., Skrutskie, M. F., et al. 2019, *PASP*, **131**, 055001

³⁹ <http://irtfweb.ifa.hawaii.edu/~spex/overview/overview.html>